JGR Oceans

RESEARCH ARTICLE
10.1029/2019JC014988

Shelf-Basin Interactions and Water Mass Residence Times in the Western Arctic Ocean: Insights Provided by Radium Isotopes

Lauren E. Kipp[1,2], David C. Kadko[3], Robert S. Pickart[4], Paul B. Henderson[2], Willard S. Moore[5], and Matthew A. Charette[2]

[1]Ocean Frontier Institute, Dalhousie University, Halifax, Nova Scotia, Canada, [2]Department of Marine Chemistry and Geochemistry, Woods Hole Oceanographic Institution, Woods Hole, MA, USA, [3]Applied Research Center, Florida International University, Miami, FL, USA, [4]Department of Physical Oceanography, Woods Hole Oceanographic Institution, Woods Hole, MA, USA, [5]Department of Earth and Ocean Sciences, University of South Carolina, Columbia, SC, USA

Abstract Radium isotopes are produced through the decay of thorium in sediments and are soluble in seawater; thus, they are useful for tracing ocean boundary-derived inputs to the ocean. Here we apply radium isotopes to study continental inputs and water residence times in the Arctic Ocean, where land-ocean interactions are currently changing in response to rising air and sea temperatures. We present the distributions of radium isotopes measured on the 2015 U.S. GEOTRACES transect in the Western Arctic Ocean and combine this data set with historical radium observations in the Chukchi Sea and Canada Basin. The highest activities of radium-228 were observed in the Transpolar Drift and the Chukchi shelfbreak jet, signaling that these currents are heavily influenced by interactions with shelf sediments. The ventilation of the halocline with respect to inputs from the Chukchi shelf occurs on time scales of ≤19–23 years. Intermediate water ventilation time scales for the Makarov and Canada Basins were determined to be ~20 and >30 years, respectively, while deep water residence times in these basins were on the order of centuries. The radium distributions and residence times described in this study serve as a baseline for future studies investigating the impacts of climate change on the Arctic Ocean.

Plain Language Summary The rapid rate of climate change in the Arctic is impacting the exchange of elements between the continental shelf and the Arctic Ocean. Radium isotopes are naturally produced in sediments and are added to the ocean when water comes into contact with the seafloor, so they are useful for identifying shelf- or sediment-influenced water parcels in the open ocean. Once removed from their sediment source, these radioactive isotopes decay at known rates and can therefore be used to determine the time elapsed since water was in contact with the shelf, or to estimate the time a water parcel spends in a certain region of the ocean. In this study, we use the levels of radium measured in the Western Arctic Ocean to determine how rapidly water moves from the surrounding shelf seas into the open Arctic Ocean, and to estimate how long water resides in the deepest parts of the Western Arctic Ocean. These time scales provide important baseline estimates that can be used in future studies to assess how climate change is affecting sediment-ocean interactions in the Arctic.

Key Points:
- Water originating over the Chukchi shelf replenishes the Canadian Basin halocline on time scales less than ~20 years
- Intermediate water ventilation time scales with respect to shelf inputs are ~20 and >30 years in the Canada and Makarov Basins, respectively
- The first measurements of radium-226 in the deep Canadian Basin indicate deep water residence times on the order of centuries

Supporting Information:
- Supporting Information S1
- Table S1

Correspondence to:
L. E. Kipp,
lkipp@whoi.edu

Citation:
Kipp, L. E., Kadko, D. C., Pickart, R. S., Henderson, P. B., Moore, W. S., & Charette, M. A. (2019). Shelf-basin interactions and water mass residence times in the Western Arctic Ocean: insights provided by radium isotopes. *Journal of Geophysical Research: Oceans*, *124*. https://doi.org/10.1029/2019JC014988

Received 22 JAN 2019
Accepted 20 APR 2019
Accepted article online 26 APR 2019

1. Introduction

The Arctic Ocean is strongly influenced by continental inputs. Over 50% of the area of this ocean is dominated by continental shelves (Jakobsson, 2002), and although it contains only 1% of the ocean volume, the Arctic basin receives over 10% of global river discharge (Aagaard & Carmack, 1989; McClelland et al., 2012). Currently, terrestrial influences on the Arctic are increasing as a result of climate change. The loss of sea ice over continental shelves allows increased coastal erosion (Günther et al., 2013) and vertical mixing (Carmack & Chapman, 2003; Rainville & Woodgate, 2009; Williams & Carmack, 2015), which may be contributing to intensified shelf-derived material fluxes to the central Arctic (Kipp et al., 2018; Rutgers van der Loeff et al., 2018). Rising temperatures are also leading to increased river discharge (Peterson et al., 2002; Rawlins et al., 2010) and permafrost degradation (Luo et al., 2016). As permafrost has historically been considered a barrier to submarine groundwater discharge (SGD) in the Arctic, this degradation may result in larger SGD inputs to the coastal ocean

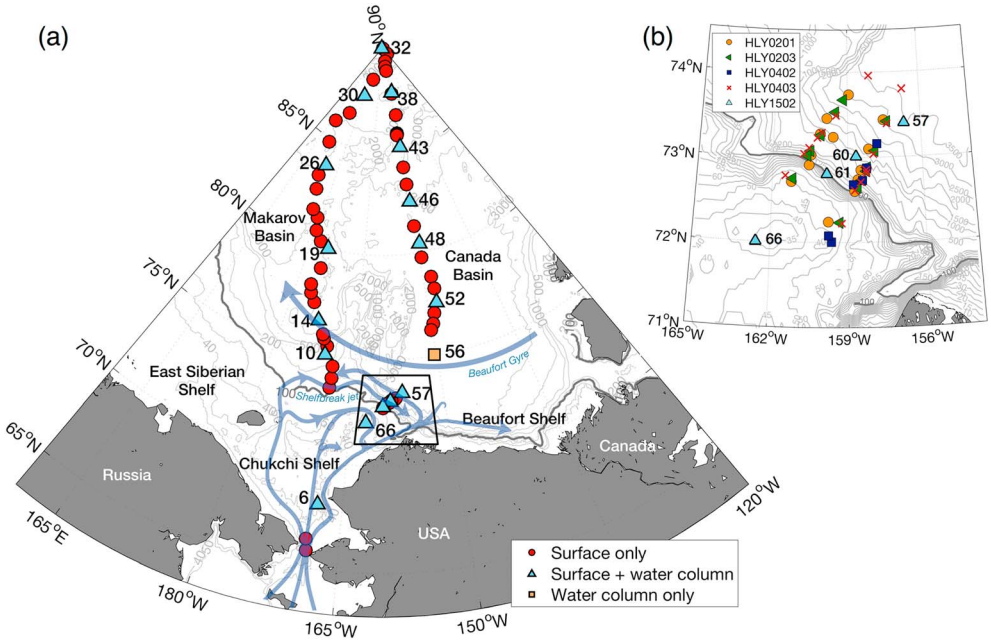

Figure 1. (a) Locations sampled on the HLY1502 northbound (stations 7–32) and southbound (stations 32–66) transects. Surface samples were collected at all stations except station 56, and water column samples were collected from selected stations. Station locations and bottom depths are listed in Table S1. The black box shows the bounds of inset (b). General circulation features (based on Corlett and Pickart, 2017) are shown in blue arrows. (b) Locations near the Chukchi shelf break sampled on the HLY1502, HLY0201, HLY0203, HLY0402, and HLY0403 expeditions. Only HLY1502 stations with water column data are included for clarity.

(Walvoord et al., 2012). It is vital to understand the modern Arctic Ocean so that we may predict how it will be impacted by these changing continental inputs.

River runoff and ice melt contribute to a fresh, cold surface water layer (typically 10–50 m thick) extending over the Arctic basin. In the Western Arctic, this layer is underlain by Pacific inflow through the Bering Strait, which becomes modified by interactions with sediments during transit over the Chukchi shelf (e.g., Carmack & Wassmann, 2006; Pickart et al., 2016). Seasonal warming and cooling, brine formation, and changing flow paths result in distinct temperature and salinity characteristics that can be used to distinguish the modified water masses in the Chukchi Sea. Chukchi winter water (WW) forms as a result of brine rejection from late fall to early spring (Muench et al., 1988; Weingartner et al., 1998; Woodgate et al., 2005). This water mass is cold, saline, and becomes enriched in sediment-derived materials, including regenerated nutrients and trace metals, through water column convection induced by brine rejection (Arrigo et al., 2017; Lowry et al., 2015; Pacini et al., 2016; Pickart et al., 2016; Vieira et al., 2018). In the summer, solar heating of this water mass transforms it into remnant winter water (RWW; Gong & Pickart, 2016). Alaskan Coastal Water (ACW) is the warmest water in the Chukchi Sea (Paquette & Bourke, 1974; Woodgate et al., 2005); this water mass originates in the Gulf of Alaska from continental runoff and is advected northward in the Alaskan Coastal Current. As such, it is influenced by Yukon River outflow and possibly groundwater inputs. Bering Summer Water (BSW) is a mixture of Anadyr water and central Bering shelf water (e.g., Pisareva et al., 2015), and is typically colder and saltier than the ACW (Shimada et al., 2001).

Observational and modeling studies suggest that these Chukchi water masses typically transit the shelf through one or more of three pathways: the eastern pathway (the Alaskan Coastal Current) follows the coast of Alaska and flows through Barrow Canyon, the central pathway progresses northward between Herald and Hanna Shoals and also feeds Barrow Canyon, and the western pathway flows through Herald Canyon (Pickart et al., 2016; Spall, 2007; Weingartner et al., 2005, 1998). These general circulation features are shown in Figure 1a. Some of the water that flows through Herald Canyon travels along the Chukchi shelfbreak from west to east, forming a shelfbreak jet (Corlett & Pickart, 2017; Li et al., 2019; Mathis et al., 2007; Pickart et al., 2010, 2005). Recently, it was discovered that much of the outflow from Barrow

Canyon is steered to the left and forms the westward flowing Chukchi Slope Current, offshore of the shelfbreak jet (Corlett & Pickart, 2017; Li et al., 2019; Spall et al., 2018). Eddies transporting shelf-influenced waters into the Canada Basin are also common (Mathis et al., 2007; Muench et al., 2000; Pickart et al., 2005; Spall et al., 2008; Timmermans et al., 2008).

Beneath the halocline, intermediate waters are ventilated by Atlantic inflows from the Eurasian Basin. Brine rejection on the shelves contributes to deep water formation (Aagaard et al., 1981; Rudels et al., 1994), transporting continentally influenced Atlantic water to intermediate depths. The movement of deep waters is restricted by bathymetry: the Lomonosov Ridge splits the Arctic into the Canadian (also referred to as Amerasian) and Eurasian Basins. The Fram Strait connects the Eurasian Basin and the North Atlantic and provides the sole deep water exchange pathway in the Arctic; thus, deep waters in the Canadian Basin are generally isolated below the sill depth of the Lomonosov Ridge (~1,700 m) and have longer residence times than those in the Eurasian Basin (Schlosser et al., 1997; Tanhua et al., 2009). The Alpha-Mendeleyev Ridge further divides the Canadian Basin into the Canada and Makarov Basins, while the Gakkel Ridge acts as a barrier between the Amundsen and Nansen Basins in the Eurasian Basin.

Radium isotopes are constantly produced through the decay of thorium in sediments and are soluble in seawater, so they act as tracers of continental and benthic inputs to the open ocean and are particularly useful in the shelf-dominated Arctic Ocean. Once removed from their sediment source, radium isotopes decay with their respective half-lives, and thus can be used to determine time scales of water transport and residence times. The two short-lived isotopes of radium, ^{223}Ra ($t_{1/2}$ = 11.4 days) and ^{224}Ra ($t_{1/2}$ = 3.66 days), can be used to identify coastal inputs and determine time scales of nearshore mixing (Moore, 2000b, 2000a). Few studies to date have utilized the short-lived Ra isotopes in the Arctic. Kadko and Muench (2005) reported high ^{224}Ra activities over the Chukchi shelf but not seaward of the shelfbreak, reflecting slow exchange between the Chukchi Sea and Beaufort Gyre. Radium-224 activities have also been used to identify eddies near the Chukchi shelf and in the Beaufort Sea (Kadko et al., 2008; Kadko & Muench, 2005).

The two longer-lived isotopes of radium, ^{228}Ra ($t_{1/2}$ = 5.75 years) and ^{226}Ra ($t_{1/2}$ = 1,600 years), have appropriate half-lives for tracing shelf inputs to the water column and for determining the residence times of deep waters, respectively (Kadko & Aagaard, 2009; Rutgers van der Loeff et al., 1995, 2012, 2018; Smith et al., 2003; Vieira et al., 2018). Radium-228 was first established as a tracer of shelf inputs in the Arctic by Rutgers van der Loeff et al. (1995). These authors observed elevated ^{228}Ra activities in surface waters over the Lomonosov Ridge and concluded that the Ra-enriched water had been transported from the Eurasian shelves via the Transpolar Drift. High ^{228}Ra activities in the Transpolar Drift have since been observed during other expeditions (Rutgers van der Loeff et al., 2012; Smith et al., 2003), and have risen in recent years, signaling increased shelf-basin interaction (Kipp et al., 2018; Rutgers van der Loeff et al., 2018).

Radium-228 enrichments have also been used to identify recently ventilated intermediate waters in the Arctic (Kadko & Aagaard, 2009; Rutgers van der Loeff et al., 1995). Due to its sediment source, Rutgers van der Loeff et al. (1995) noted the usefulness of using ^{228}Ra as a tracer of intermediate waters formed via brine rejection and shelf outflows. Based on ^{228}Ra/^{226}Ra activity ratios, Kadko and Aagaard (2009) recorded inputs from both the Eurasian and Chukchi shelves in the Canada Basin halocline, and estimated a transit time of 5–7 years for Pacific inflow to reach the interior Canada Basin. Most recently, elevated ^{228}Ra activities between 1,000 and 1,500 m in the Amundsen Basin were used to determine a ventilation time scale of 15–18 years (Rutgers van der Loeff et al., 2018).

Radium-226 accumulates in deep water masses as a result of the remineralization of sinking particles and diffusion of newly produced ^{226}Ra from benthic sediments (Broecker et al., 1976; Chan et al., 1976; Chung & Craig, 1980). These two sources can theoretically be separated by employing another remineralization tracer, such as silica (Si) or barium (Ba), and the accumulation of ^{226}Ra from benthic inputs can then be used to determine water mass residence times. Relatively small sediment enrichments (Broecker et al., 1976) and variability of the Ra-Ba-Si relationships over basin-wide scales (Chung, 1980) preclude the use of this method in most ocean basins. However, the long water residence times in the small, enclosed Arctic Canadian Basin result in significant accumulation of "new" benthic-sourced ^{226}Ra, and this tracer was recently applied to estimate a deep water residence time of ~550 years in the Makarov Basin (Rutgers van der Loeff et al., 2018).

Here we present the most extensive data set of radium isotopes in the Western Arctic to date. We apply these tracers to identify significant shelf inputs to the water column and determine intermediate water ventilation time scales and deep water residence times in the Makarov and Canada Basins.

2. Methods

2.1. Sample Collection

Samples were collected between Dutch Harbor, Alaska, and the North Pole during the U.S. GEOTRACES Arctic expedition on the *USCGC Healy* from 6 August to 10 October 2015 (HLY1502, GN01). The northbound transect (stations 1–32; Figure 1a and Table S1) sampled the Bering Sea, Bering Strait, and Chukchi Shelf, and then crossed the Mendeleyev Ridge into the Makarov Basin, following the 180°W meridian. The southbound transect (stations 32–66) crossed the Alpha Ridge into the Canada Basin, generally following the 150°W meridian between 75°N and 90°N, before crossing back over the Chukchi shelf just west of Barrow Canyon. In this manuscript we include only the data collected north of the Bering Strait (stations 4–66); the results of the Bering Sea sampling will be discussed elsewhere.

Surface water samples were collected with a deck-mounted pump with an intake hose deployed at 2 m below the sea surface. Approximately 280 L of water was pumped into plastic barrels then filtered at <1 L/min through an acrylic fiber coated with manganese oxide (MnO_2), which quantitatively scavenges Ra isotopes. For shelf stations, the water was first filtered through a 1-μm Hytrex cartridge filter to remove particles that would otherwise clog the Mn fiber and increase sample processing times.

Water column samples were collected using McLane in situ pumps deployed on a plastic-coated Vectran line. Pumps were programmed to operate for 4 hr at the target depths, typically filtering 1,200–1,600 L for each sample at an average flow rate of 5.6 L/min. Water was first passed through a series of filters to collect small (<51 μm) and large (>51 μm) particles, and then through a cellulose cartridge coated with MnO_2 to collect dissolved Ra, Th, and Ac isotopes (Henderson et al., 2013). The cartridge collection efficiencies were determined using small-volume (15–20 L) samples collected at corresponding depths. These samples were collected from Niskin bottles either mounted on the conductivity-temperature-depth rosette (shallow casts, typically <1,000 m) or above the in situ pumps (deep casts, typically >1,000 m), and were filtered through Mn fiber.

2.2. Sample Analysis

After collection, filters and cartridges were rinsed with Ra-free deionized water to remove any particles and then partially dried with filtered, compressed air. Short-lived Ra isotopes were analyzed on the ship within three days of collection using Radium Delayed Coincidence Counting (RaDeCC), which measures the activities of ^{223}Ra and ^{224}Ra through the alpha decay of their respective daughter isotopes, ^{219}Rn and ^{220}Rn (Moore & Arnold, 1996). Radium-223 and ^{224}Ra are produced through the decay of ^{227}Ac ($t_{1/2}$ = 21.8 years) and ^{228}Th ($t_{1/2}$ = 1.91 years), respectively. Actinium-227 is soluble in seawater, while ^{228}Th is particle reactive. Due to their short half-lives, the offshore activities of ^{223}Ra and ^{224}Ra are mainly supported by the decay of ^{227}Ac and ^{228}Th in seawater; thus, it is useful to differentiate between total activities ($^{223}Ra_{tot}$ and $^{224}Ra_{tot}$) and unsupported, or excess, activities ($^{223}Ra_{xs}$ and $^{224}Ra_{xs}$). To determine supported activities, dissolved ^{227}Ac and ^{228}Th were measured on the cartridges and particulate ^{228}Th was measured on the filters that preceded the cartridges on the McLane pump flow path. These analyses were made using RaDeCC after allowing the unsupported ^{223}Ra and ^{224}Ra to decay to negligible activities. Water column $^{224}Ra_{xs}$ activities were then determined by subtracting the measured activities of dissolved + particulate ^{228}Th from $^{224}Ra_{tot}$, and $^{223}Ra_{xs}$ was determined by subtracting dissolved ^{227}Ac from $^{223}Ra_{tot}$. Actinium-227 and particulate ^{228}Th were not measured in surface samples, so $^{223}Ra_{xs}$ is not reported for these samples and $^{224}Ra_{xs}$ represents $^{224}Ra_{tot}$ minus dissolved ^{228}Th only. The RaDeCC measurement efficiency was determined using a set of fiber, cartridge, and filter standards (Henderson et al., 2013; Maiti et al., 2015). The analyses of the short-lived isotopes and ^{228}Th were shared between the Moore lab at the University of South Carolina and the Charette lab at the Woods Hole Oceanographic Institution, and ^{227}Ac was measured by the Hammond lab at the University of Southern California. All three groups participated in a GEOTRACES intercalibration experiment (Charette et al., 2012) and regularly exchange standards to ensure that the measurements of all four radium isotopes are consistent between the labs.

After RaDeCC analysis, fibers and cartridges were ashed in a muffle furnace at 820 °C for 12 and 48 hr, respectively. The ash was packed into polystyrene vials, sealed with epoxy to prevent ^{222}Rn loss, and aged for at least three weeks to allow daughter isotopes to reach equilibrium. Samples were analyzed on high-purity well-type germanium detectors; surface samples were analyzed in the Moore lab and water column samples were analyzed in the Charette lab. Radium-228 was measured using the lines of ^{228}Ac (338 and 911 keV) and ^{226}Ra was measured using the line for ^{214}Pb (352 keV). Detector efficiencies were determined using a set of ashed standards spiked with ^{226}Ra and ^{232}Th with daughters in equilibrium and prepared in the same way as the samples.

The ^{226}Ra activities of the small volume samples were analyzed using an alpha scintillation technique described by Key et al. (1979). Briefly, fibers were sealed in 125-mL PVC housings for a minimum of three weeks to allow ^{222}Rn to reach equilibrium with its parent ^{226}Ra. The ^{222}Rn was then purged from the housing with helium at a flow rate of 250 mL/min and trapped in a cryo-loop cooled with liquid nitrogen. After purging for 15 min, the cryo-loop was isolated and heated, and the trapped ^{222}Rn was transferred to an alpha scintillation (Lucas) cell to be analyzed on a radon counting system (Model AC/DC-DRC-MK 10-2). Samples were analyzed for ~230 min, resulting in counting uncertainties of <8%. The ^{226}Ra measurement efficiency was determined using fiber standards containing 20 dpm ^{226}Ra (NIST SRM#4967A) that were analyzed the same way as the samples.

The ^{226}Ra activities measured on the small volume samples were compared to those on the cartridges collected from the corresponding depths in order to determine the Ra collection efficiencies. The collection efficiency of individual cartridges ranged from 19 to 99%, with an average of 70 ± 19% (1σ; n = 224). Variability in the collection efficiency may be related to differences in flow rate or in the cartridge seating in the sampling setup, but because there is an efficiency measurement for each individual cartridge this range does not add uncertainty to the final Ra activities. The errors on the individually determined cartridge collection efficiencies were propagated with counting errors to produce the errors on the reported activities.

2.3. Sampling Procedures for Historical Data Sets

In addition to the samples collected on the 2015 HLY1502 transect, we also present Ra data collected during the Western Arctic Shelf-Basin Interactions (SBI) expeditions on the *USCGC Healy* (HLY0201, 6 May to 14 June 2002; HLY0203, 17 July to 26 August 2002; HLY0402, 15 May to 23 June 2004; HLY0403, 19 July to 25 August 2004; HLY0404, 2–30 September 2004), the Arctic West Summer (AWS) 2000 expedition on the *USCGC Polar Star* (hereafter referred to as AWS-2000; 27 July to 21 September 2000), and the 1998 Surface Heat Budget of the Arctic Ocean (SHEBA) ice camp (Tables S2–S4). Some of the SBI data have been previously published, and a detailed description of sampling and analytical methods for these expeditions can be found in Kadko et al. (2008) and Kadko and Muench (2005). Sampling on the other expeditions was conducted in the same manner.

3. Results

3.1. Radium-223 and Radium-224

Surface water $^{224}Ra_{xs}$ activities (corrected for dissolved ^{228}Th but not particulate ^{228}Th; see section 2) were ~3 dpm/100 L in the Bering Strait and <1 dpm/100 L for most of the northbound transect (Figure S1). Near the North Pole, surface water activities increased to 4.5 dpm/100 L, and remained between 1 and 3 dpm/100 L for much of the southbound transect. Excess ^{224}Ra activities were 1–2 dpm/100 L in surface waters over the Chukchi shelf and up to 3 dpm/100 L on the southbound shelf crossing, but were <1 dpm/100 L on the northbound shelf crossing. Water column $^{224}Ra_{xs}$ activities (corrected for both dissolved and particulate ^{228}Th) were generally <0.4 dpm/100 L, with the exception of a few samples in the halocline on the southbound transect that had activities between ~0.5 and 1.5 dpm/100 L, and a sample collected over the Chukchi shelf with an activity of 2.2 ± 0.4 dpm/100 L (station 66; Figures S2 and S3). Bottom water enrichments indicate benthic inputs in the Makarov and Amundsen Basins (stations 30 and 32), over the Alpha Ridge (station 46), and near the Chukchi slope (stations 57 and 60; Figure S3).

Total ^{223}Ra activities were <0.1 dpm/100 L in surface waters north of 70°N, while activities in the Bering Strait and over the southern Chukchi Shelf were ~0.3–0.45 dpm/100 L Figure (S4). Open ocean water column $^{223}Ra_{xs}$ activities were below 0.15 dpm/100 L, while higher activities were measured on the

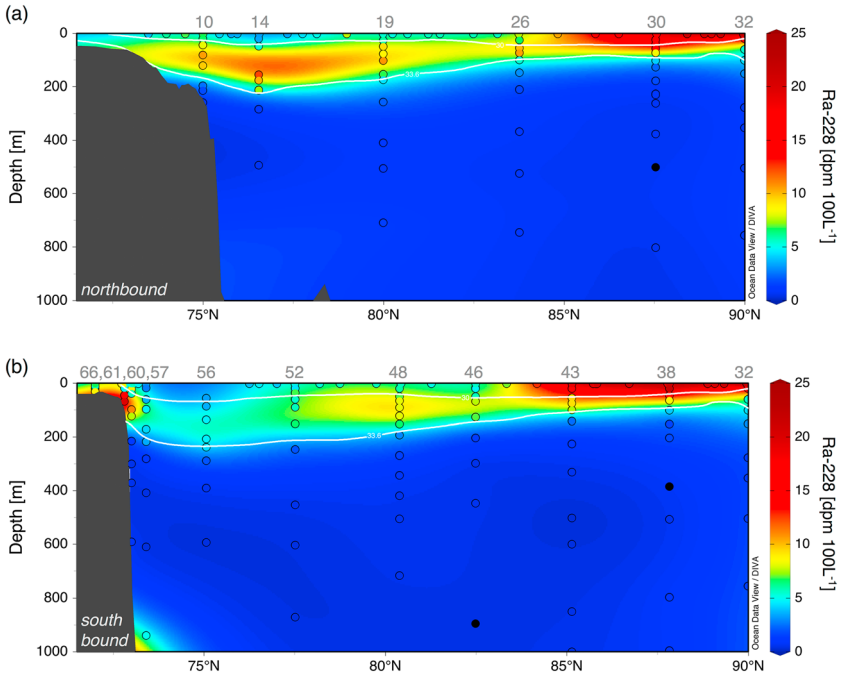

Figure 2. Vertical sections of ^{228}Ra activities for the (a) northbound and (b) southbound HLY1502 transects. Colored symbols indicate measured activities, and background shading represents interpolated activities calculated with Ocean Data View's View's DIVA gridding software. Black symbols indicate samples below the detection limit. White contours indicate salinities 30 and 33.6, denoting the boundaries of the shelf-modified Pacific inflow. Station numbers are listed in grey.

southbound shelf crossing (0.30–0.35 dpm/100 L; Figure S5) and over the Chukchi Shelf (0.25–0.56 dpm/100 L; station 6). Benthic inputs were apparent near the Alpha Ridge (stations 38, 43, 46, 48) and in the Amundsen Basin (station 32; Figure S5).

3.2. Radium-228

Radium-228 activities in Arctic surface waters are some of the highest in the open ocean due to the strong continental influence in this basin. The ^{228}Ra activities measured at the surface on the HLY1502 transect ranged from 3 to 23 dpm/100 L (Figures 2 and S6). By comparison, the highest activities in Atlantic and Pacific surface waters are typically below 5 and 1 dpm/100 L, respectively (Charette et al., 2015; Sanial et al., 2018). The highest ^{228}Ra activities on the HLY1502 transect (~23 dpm/100 L) were observed between 85°and 90°N from the surface to approximately 50 m (Figure 2), and were associated with meltwater and meteoric water (MW) at a temperature of −1.5 °C and salinity of ~28 (Figure S7). These samples were collected in the Transpolar Drift (see section 4.2.1). Minimum values in surface water (~3–4 dpm/100 L) were observed near 77°N on the northbound transect and 75°N on the southbound transect, and also fall in the T-S space occupied by MW (Figure S7).

Activities were generally 5–15 dpm/100 L in the shelf-modified Pacific layer and were elevated (up to 20 dpm/100 L) near the Chukchi shelfbreak, particularly on the southbound transect. These elevated activities were associated with WW and RWW (Figure S7). The apparent difference between the two shelf crossings may simply be due to the higher sampling resolution on the southbound transect, which allowed samples to be collected closer to the shelfbreak and slope. Below the halocline, activities were below 5 dpm/100 L, reflecting the isolation of deeper waters from the shelf source of ^{228}Ra (Figures S6–S8). There was a midwater column enrichment in ^{228}Ra (up to 2 dpm/100 L) between 500 and 1,500 m evident in the Makarov Basin, particularly at station 19 over the Mendeleyev Ridge, and at station 32 in the Amundsen Basin (Figures 3 and S9). A similar pattern was not observed in Canada Basin intermediate waters. Some samples were below detection, particularly in the deep Canada Basin (Figure S8). A few stations showed influence of benthic inputs, with activities near the bottom increasing up to ~1 dpm/100 L.

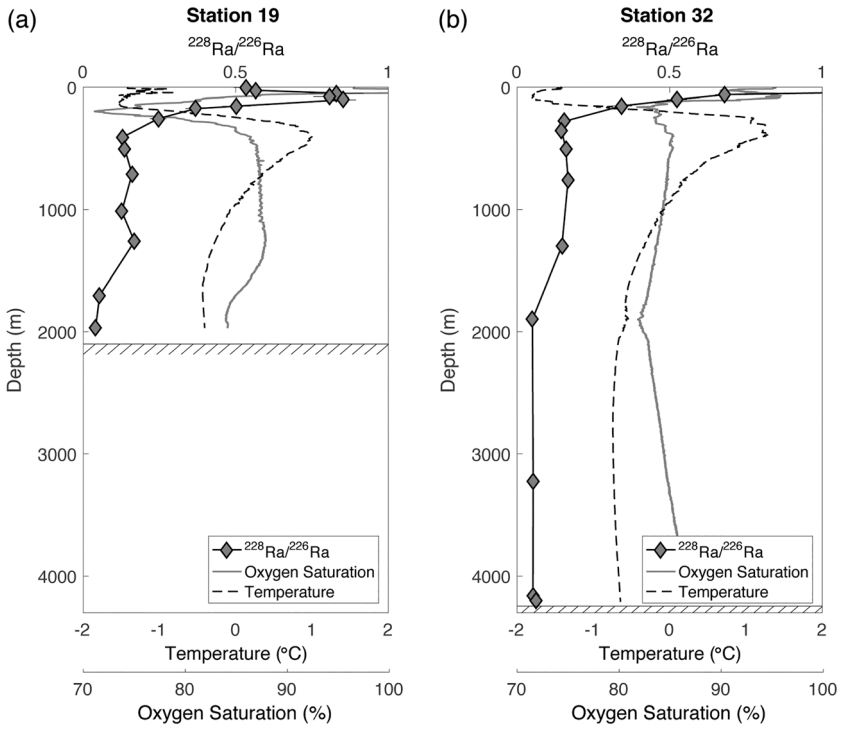

Figure 3. Depth profiles of the $^{228}Ra/^{226}Ra$ activity ratios, oxygen saturation, and temperature at (a) station 19, located over the Mendeleyev Ridge, and (b) station 32, located in the Amundsen Basin. Oxygen saturation was calculated using the equations in Weiss (1970) and the oxygen concentrations, temperatures, and salinities reported by Landing et al. (2016).

These inputs were particularly evident at stations 14 (in the Chukchi Abyssal Plain), 30 (in the Makarov Basin), and 43 and 46 (above the Alpha Ridge). Bottom water values at the other stations were ~0.5 dpm/100 L. Benthic ^{228}Ra activities in the Arctic were similar to those observed in the Atlantic (0.5–1.0 dpm/100 L; Charette et al., 2015), but higher than those in the Pacific (<0.6 dpm/100 L), where activities are low due to dilution and decay in the large Pacific Basin (Sanial et al., 2018).

3.3. Radium-226

Radium-226 activities were lowest in the fresh surface MW layer, ranging between 7 and 10 dpm/100 L (Figures 4, S7, and S10). Activities were higher (up to 14 dpm/100 L) in the shelf-modified Pacific inflow; these activities are similar to those observed in the upper 1,000 m of the North Pacific (Chung & Craig, 1980). Similar to ^{228}Ra, the elevated ^{226}Ra activities were associated with WW, RWW, and cold MW carried in the Transpolar Drift (Figure S7). Activities were below 10 dpm/100 L in the Atlantic layer between approximately 500 and 1,500 m, and then increased with depth. The deep Makarov and Canada Basins had the highest ^{226}Ra activities, reaching up to 17 dpm/100 L (Figures 4, S7, and S10). To the best of our knowledge, this study presents the first measurements of ^{226}Ra below 2,000 m in the Canada Basin. The activities measured at the sole Eurasian Basin station (station 32) were lower, with a maximum of 12 dpm/100 L. These deep water values fall between those observed in the North Atlantic (~9–12 dpm/100 L; Broecker et al., 1976) and North Pacific (~30–36 dpm/100 L; Chung & Craig, 1980).

4. Discussion

4.1. Short-Lived Radium Isotopes in the Arctic Basin

Excess ^{223}Ra and ^{224}Ra will decay to negligible activities in ~60 and ~20 days, respectively, after removal from their sediment source. The low water column activities of $^{223}Ra_{xs}$ and $^{224}Ra_{xs}$ observed in the Arctic basin are consistent with this loss via decay, while elevated activities in bottom waters reflect inputs from benthic sediments (Figures S2, S3, and S5). Higher activities of $^{224}Ra_{xs}$ were observed in the water column

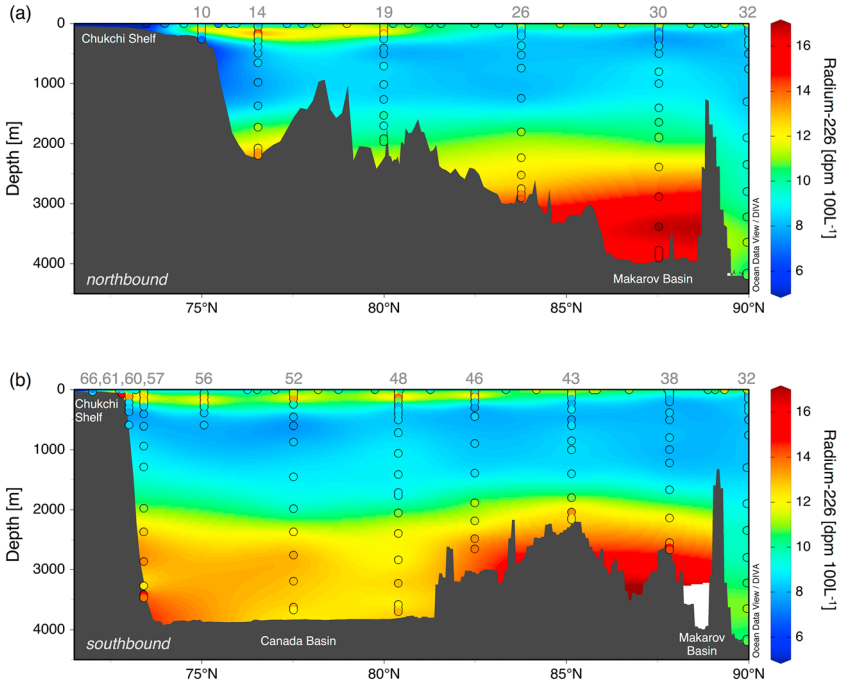

Figure 4. Vertical sections of ^{226}Ra activities on the (a) northbound and (b) southbound HLY1502 transects. Colored symbols indicate measured activities, and background shading represents interpolated activities calculated with Ocean Data View's DIVA gridding software. Station numbers are listed in grey.

on the southbound transect, while most of the activities on the northbound transect were below detection; we do not currently have an explanation for this difference between the Canada and Makarov Basins. The activities of $^{224}Ra_{xs}$ in surface waters far from the coast are surprisingly high, up to 3–4.5 dpm/100 L in the Transpolar Drift (Figure S1). The water carried in the Transpolar Drift left the shelf a minimum of six months prior to our sampling (Kipp et al., 2018), and thus should have no remaining shelf-sourced $^{224}Ra_{xs}$. Eddies have been shown to transport $^{224}Ra_{xs}$ up to 200 km from the shelf in the Canada Basin (Kadko & Muench, 2005), but it is unlikely that eddies could explain the presence of $^{224}Ra_{xs}$ as far north as 85°N, over 1,000 km from the shelf. Further, the lack of ^{223}Ra anomalies at the same locations as the high $^{224}Ra_{xs}$ indicates that eddies, which would transport both isotopes, cannot fully explain the presence of $^{224}Ra_{xs}$ (Figures S1 and S4).

The surface $^{224}Ra_{xs}$ activities were corrected for dissolved ^{228}Th but particulate ^{228}Th was not measured on these samples; thus, some of the $^{224}Ra_{xs}$ is likely supplied from particulate ^{228}Th. For stations north of 75°N, particulate ^{228}Th measured between 20 and 25 m (shallowest available estimates) was between 5 and 30% of dissolved ^{228}Th (Black, 2017). Increasing the amount of ^{228}Th subtracted from $^{224}Ra_{tot}$ by 30% accounts for the low $^{224}Ra_{xs}$ activities observed on the northbound transect, but is not enough to explain the $^{224}Ra_{xs}$ observed near the North Pole and on the southbound transect. However, particulate ^{228}Th activities at the surface may be higher than those at 20 m due to a combination of scavenging on biological particles, under-ice algae, and/or release of ice-rafted sediment; such ice-water boundary processes have been suggested to affect the shorter-lived isotope of thorium, ^{234}Th ($t_{1/2}$ = 24.1 days; Ma et al., 2005; Amiel & Cochran, 2008; Cai et al., 2010), and significant amounts of particulate ^{228}Th (0.8–2 dpm/100 L) were observed in the Transpolar Drift by Rutgers van der Loeff et al. (2018). Future studies should focus on constraining the possible influences of ice algae and ice-rafted sediment on the distributions of ^{228}Th and ^{224}Ra in Arctic surface waters.

4.2. Shelf Inputs at the Surface and in the Halocline

The strong ^{228}Ra enrichments in the surface and halocline waters are due to shelf inputs that have accumulated in this layer. Kadko and Aagaard (2009) suggested that heterogeneity in the halocline distribution of

^{228}Ra may arise from a combination of episodic shelf inputs, eddies, and downwelling. Based on the extensive data set provided by the HLY1502 and SBI expeditions, some specific shelf influences in the Western Arctic can be identified.

4.2.1. Distinct Surface Water Sources Indicated by ^{228}Ra

Radium-228 activities were highest in surface waters near the North Pole (Figure 2); this ^{228}Ra-enriched water was transported from the East Siberian and Laptev Shelf Seas via the Transpolar Drift. These wide and shallow Eurasian Seas are a large source of ^{228}Ra to the overlying waters, and are transported on time scales of 6–12 months to the central Arctic (Kipp et al., 2018). The activities observed in the Transpolar Drift in 2015 were approximately double those observed in 2007; because the shelves are the largest source of ^{228}Ra to the surface ocean, this indicates a substantial increase of shelf-derived materials to the Arctic over the last decade (Kipp et al., 2018; Rutgers van der Loeff et al., 2018).

The relatively low ^{228}Ra activities observed in surface waters near 77°N on the northbound transect and 75°N on the southbound transect are associated with low salinity (<27) and high fractions of meteoric water (>0.15; Pasqualini et al., 2017). This water is part of the southern arm of the Beaufort Gyre, which accumulates and stores river runoff (Carmack et al., 2016). The low ^{228}Ra activities result from decay during circulation in the gyre (Hansell et al., 2004; Kadko & Muench, 2005). Back trajectories determined for the ice at these sample locations showed either little movement (stations 53–55) or clockwise circulation (stations 11–16, 57), reflecting their position in the gyre, and surface water ages based on the ingrowth of ^{228}Th with its parent ^{228}Ra indicate that this water mass has been removed from the shelf for at least three years (Kipp et al., 2018).

4.2.2. Influence of the Shelfbreak Jet

The HLY1502 southbound transect and the SBI spring and summer 2002 and 2004 transects (HLY0201, HLY0203, HLY0402, HLY0403) crossed the Chukchi shelfbreak in similar locations, west of Barrow Canyon (Figures 1b and S11). These eight transects were used to compute composite mean sections of the Ra activities, temperature, salinity, and absolute geostrophic velocity across the Chukchi shelfbreak using the approach described in Corlett and Pickart (2017) (Figure 5). The composite mean plots reveal that the high ^{228}Ra activities observed near the shelfbreak are associated with cold water moving from west to east. This result, along with the ^{228}Ra enrichments observed in WW and RWW in the regional T-S diagram (Figure S7), suggests that ^{228}Ra-enriched WW is being transported from the Chukchi Shelf via the Chukchi shelfbreak jet (Corlett & Pickart, 2017; Li et al., 2019). The WW advected by the shelfbreak jet likely becomes enriched in ^{228}Ra during its residence time over the Chukchi shelf (Vieira et al., 2018). Convective overturning as a result of brine rejection during ice formation and lead refreezing can transport sediment-derived materials such as ^{228}Ra into the overlying water column (Arrigo et al., 2017; Lowry et al., 2015; Pickart et al., 2016; Vieira et al., 2018). Internal wave generation and vertical mixing during the ice-free season can also facilitate this transport (Rainville & Woodgate, 2009). Our synthesis shows that the advection of WW in the shelfbreak jet plays a key role in transporting sediment-derived materials off the Chukchi shelf via Herald Canyon. This Ra-enriched WW can subsequently be transported to the Canada Basin halocline through eddies that spawn from the shelfbreak jet (Mathis et al., 2007; Pickart et al., 2005; Spall et al., 2008). However, most of the WW likely stays in the jet all the way to Barrow Canyon where the isobaths steer the water southward into the canyon mouth. At this point the more substantial outflow from the Chukchi shelf, emanating from the head of the canyon, entrains the WW from the Chukchi shelfbreak jet and carries it offshore. This combined offshore flux then feeds both the Beaufort shelfbreak jet to the east and the Chukchi slope current to the west (Corlett & Pickart, 2017; Spall et al., 2018). The precise fate of the slope current is presently unknown, but models (e.g., Spall et al., 2018) suggest that a substantial portion of it is ultimately entrained into the Beaufort Gyre.

Activities of ^{226}Ra are also highest in the shelfbreak jet, and the elevated ^{226}Ra signal extends farther into the halocline than that of ^{228}Ra (Figure 5e). This may reflect the longer half-life of ^{226}Ra. Residence times in the halocline have been estimated to be ~3–10 years (Östlund, 1982; Östlund & Hut, 1984; Schlosser et al., 1999), which would allow a significant amount of ^{228}Ra to decay but would not measurably affect the ^{226}Ra activities. The ^{228}Ra/^{226}Ra activity ratio of the shelfbreak jet is approximately 0.9–1.1 (Figure 5f). Seasonal variability in the absolute ^{228}Ra and ^{226}Ra activities in the shelfbreak jet will be the subject of another manuscript; the spatial patterns and ^{228}Ra/^{226}Ra activity ratio were similar in all seasons with available data.

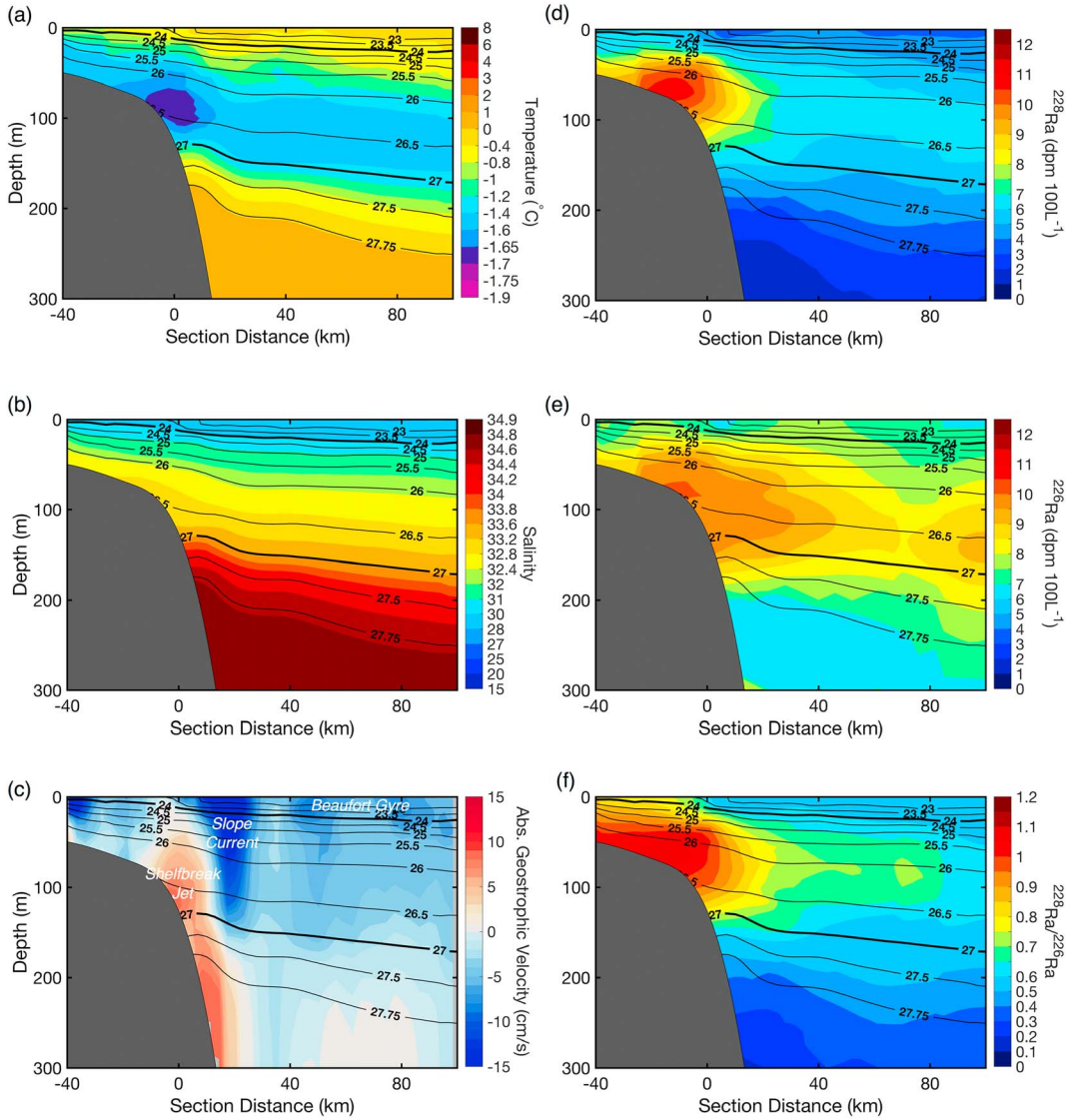

Figure 5. Composite mean vertical sections of (a) temperature, (b) salinity, (c) absolute geostrophic velocity (positive velocities are eastward), (d) ^{228}Ra activity, (e) ^{226}Ra activity, and (f) the ^{228}Ra/^{226}Ra activity ratio across the Chukchi shelf break. Isopycnals are shown in black; bold isopycnals (σ = 24, 27) denote the boundaries of the shelf-influenced Pacific inflow. Data from the Chukchi shelf crossings shown in Figure 1b were used to calculate the mean sections. Individual sampling locations are shown in Figure S11.

4.2.3. ^{228}Ra/^{226}Ra Signatures in the Halocline

The combination of strong shelf influences and decay of ^{228}Ra on subdecadal time scales leads to variability in the ^{228}Ra/^{226}Ra activity ratios observed in Western Arctic surface and halocline waters; this variability can be used to identify specific shelf inputs to the upper water column and determine the time elapsed since water was in contact with the shelf. Because of the shorter half-life of ^{228}Ra, this isotope regenerates more quickly than ^{226}Ra in sediments. This can result in ^{228}Ra/^{226}Ra activity ratios greater than 1 over continental shelves; ratios as high as 3.9 have been observed over the Laptev Shelf (Rutgers van der Loeff et al., 2003). After water leaves the shelf, residence times in the surface and halocline are long enough (~3–10 years; Östlund, 1982; Östlund & Hut, 1984; Schlosser et al., 1999) that the ^{228}Ra/^{226}Ra activity ratio will decrease due to ^{228}Ra decay. The change in the ^{228}Ra/^{226}Ra activity ratio can therefore be used to determine the time elapsed since the water mass advected off the shelf. The activity ratio is used instead of the absolute ^{228}Ra activity to correct for the effects of dilution, which will affect both isotopes to the same extent (Rutgers van der Loeff et al., 1995; Kadko & Muench, 2005).

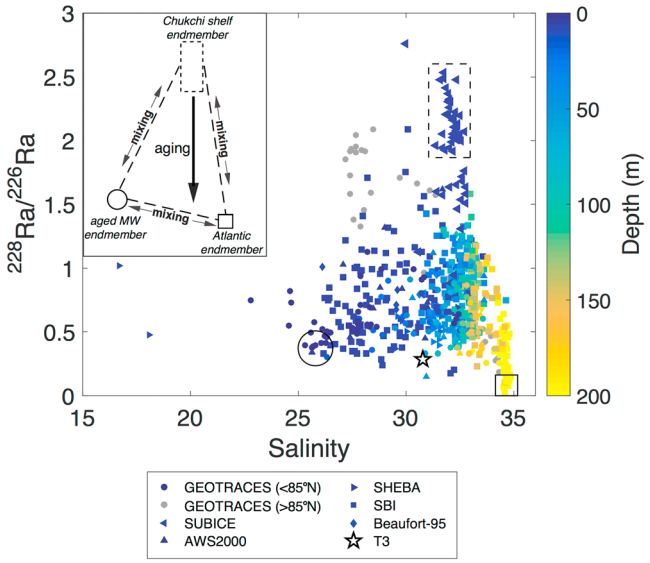

Figure 6. $^{228}Ra/^{226}Ra$ activity ratio as a function of salinity for samples collected in Western Arctic surface waters (≤200 m). Symbol color indicates depth in the water column, and symbol shape indicates the sampling expedition. For clarity, error bars are not shown. GEOTRACES samples collected above 85°N are shown in grey; these samples were collected in the Transpolar Drift and originated from the Eurasian shelf seas. The activity ratio measured at ice station T3 in 1968 (Kaufman et al., 1973) is indicated by a white star. Samples collected on the SUBICE expedition were reported by Vieira et al. (2018) and samples collected on the Beaufort-95 expedition were reported by Smith et al. (2003). The black dashed rectangle represents the Chukchi shelf end-member, the black circle denotes the aged meteoric and meltwater end-member, and the black square indicates the Atlantic water end-member (see section 4.2.3). Inset shows the relative positions of end-members in $^{228}Ra/^{226}Ra$-salinity space. Dashed lines indicate mixing between the end-members, and the vertical arrow shows the effect of aging on the $^{228}Ra/^{226}Ra$ activity ratio.

However, this calculation can be biased by mixing between water masses with different $^{228}Ra/^{226}Ra$ signatures. The upper water column in the Western Arctic contains multiple end-members: water recently in contact with the shelf (including ACW, BSW, RWW, and WW), fresh MW, and saline AW beneath the halocline. Shelf water has high $^{228}Ra/^{226}Ra$ activity ratios, and is typically associated with low salinities due to river inputs over shelves (Rutgers van der Loeff et al., 2003; Smith et al., 2003). The MW end-member has low $^{228}Ra/^{226}Ra$ ratios due to ^{228}Ra decay during circulation in the Beaufort Gyre, and low salinities due to ice melt and river discharge. The $^{228}Ra/^{226}Ra$ activity ratio of 0.29 measured at the T3 ice station in the Canada Basin in 1968 (Kaufman et al., 1973) is often used to represent the aged MW end-member (Rutgers van der Loeff et al., 1995; Smith et al., 2003; Kadko & Muench, 2005). The AW end-member represents saline water deeper in the halocline that has low $^{228}Ra/^{226}Ra$ activity ratios (<0.2) due to decay.

The $^{228}Ra/^{226}Ra$ activity ratios measured in the upper 200 m of the Western Arctic over the last two decades range between ~0 and 2.5 and generally fall within salinities of 23–35 (Figure 6). The compilation of data sets presented here allows for a more robust analysis of the Western Arctic surface and halocline end-members than was possible in previous studies. The HLY1502 transect included many measurements in the Canada Basin, capturing the aged MW end-member. This low-salinity water mass was measured in samples collected between stations 53 and 57 (73.4°–77.0°N), which displayed $^{228}Ra/^{226}Ra$ activity ratios of 0.30–0.46 at salinities of 25.30–26.34; several samples from the AWS2000 and SBI expeditions fell within this range as well (black circle on Figure 6). The activity ratio of this newly defined MW end-member is similar to that of the T3 ice station, but with a lower salinity. This is likely due to freshening of Arctic surface waters over the last few decades (Swift et al., 2016). The HLY1502 transect also provided high-resolution water column measurements that can be used to determine the signature of AW. This end-member was determined by taking the mean of HLY1502 samples with temperatures <1 °C and salinities >34 (n = 143); this resulted in an average $^{228}Ra/^{226}Ra$ activity ratio of 0.064 and an average salinity of 34.86 (black square in Figure 6).

As mentioned above, previous studies have identified the shelf end-member through high $^{228}Ra/^{226}Ra$ activity ratios and low salinities (Rutgers van der Loeff et al., 1995; Smith et al., 2003). The lack of a direct freshwater input to the Chukchi Sea precludes the use of this approach here; however, a recent study conducted in the Chukchi Sea in spring 2014 sampled distinctly high $^{228}Ra/^{226}Ra$ activity ratios (SUBICE expedition; Vieira et al., 2018). These high values reflect ^{228}Ra addition through recent water column convection as a result of winter overturning and ice lead refreezing in the spring; this convection facilitates the transport of ^{228}Ra produced in shelf sediments into the overlying water column (Vieira et al., 2018). We use the range of activity ratios measured in this study as our Chukchi shelf end-member (dashed rectangle in Figure 6). Because the water on the shelf at this time of year is composed of WW and RWW, this can also be considered a WW end-member. The cluster of HLY1502 samples with $^{228}Ra/^{226}Ra$ activity ratios around 2 were collected in the Transpolar Drift (>85°N), which carries the high $^{228}Ra/^{226}Ra$–low-salinity shelf signal from the Kara and Laptev Seas (Rutgers van der Loeff et al., 1995, 2003) (shown in grey on Figure 6).

Lines drawn between end-members represent rapid mixing between them, with little ^{228}Ra decay. Water originating on the Chukchi shelf contributes to the ventilation of the upper halocline (Aagaard et al., 1981; Pickart et al., 2005; Weingartner et al., 1998), and mixing with MW and AW will modify the $^{228}Ra/^{226}Ra$ activity ratio and salinity of this water mass. The $^{228}Ra/^{226}Ra$ activity ratio of the Chukchi shelf end-member will also decrease due to decay during its residence time in the halocline. The modified ratios should fall

within the envelope defined by the mixing curves shown in Figure 6. Although ratios do not mix linearly, we assume that mixing biases do not introduce a significant amount of error because the range of ^{226}Ra activities is small compared to the range of ^{228}Ra activities in surface waters (~3–23 dpm/100 L for ^{228}Ra, ~5–15 for ^{226}Ra; Rutgers van der Loeff et al., 1995; Kadko & Muench, 2005). The mixing line drawn between the MW and AW end-members identifies the lower limit of ^{228}Ra/^{226}Ra activity ratios expected in the halocline, as this denotes mixing between two aged water masses. The difference between the ^{228}Ra/^{226}Ra activity ratio in the Chukchi Sea and the ratio at the corresponding salinity on this MW-AW line therefore represents the maximum amount of ^{228}Ra decay expected in the halocline for water originating over this shelf. This decay can be used to determine the halocline ventilation time scale with respect to inputs from the Chukchi shelf (equation (1)):

$$\left(\frac{^{228}\mathrm{Ra}}{^{226}\mathrm{Ra}}\right)_t = \left(\frac{^{228}\mathrm{Ra}}{^{226}\mathrm{Ra}}\right)_0 e^{-\lambda_{228}\cdot t} \quad (1)$$

In equation (1), $\left(\frac{^{228}\mathrm{Ra}}{^{226}\mathrm{Ra}}\right)_t$ is the activity ratio of ^{228}Ra/^{226}Ra on the MW-AW end-member mixing line determined at a given salinity, $\left(\frac{^{228}\mathrm{Ra}}{^{226}\mathrm{Ra}}\right)_0$ is the ratio of the Chukchi shelf end-member, λ_{228} is the decay constant for ^{228}Ra, and t is the time elapsed. Using the spring ^{228}Ra/^{226}Ra activity ratios measured during the SUBICE expedition as the initial ratios (1.9–2.5; Vieira et al., 2018), and the ratios on the MW-AW line at corresponding salinities of 31.3–32.7 as the minimum expected ratios in the halocline (0.15–0.20), the halocline ventilation time scale was determined to be 19–23 years. Because the MW-AW mixing line represents the lower limit of expected ^{228}Ra/^{226}Ra ratios in the halocline, and the spring ^{228}Ra/^{226}Ra activity ratios represent the upper limit of expected ratios over the shelf, this estimate is an upper limit of the halocline ventilation time scale. Many samples fall above the MW-AW mixing line, indicating that less ^{228}Ra has decayed and less time has elapsed.

The six data sets compiled for this analysis span two decades and exhibit similar relationships between ^{228}Ra/^{226}Ra activity ratios, salinity, and depth. The ventilation time scale of ≤19–23 years is thus likely to be representative for Chukchi shelf inputs to the Canada Basin halocline between 1995 and 2015. However, rising ^{228}Ra activities in the Transpolar Drift indicate that climate change has impacted Ra inputs from the Eastern Arctic shelves over the last decade (Kipp et al., 2018; Rutgers van der Loeff et al., 2018). This change is likely driven by intensified wind-driven vertical mixing as a result of an increased number of open water days over the Laptev and East Siberian Seas. Although there was not a significant change in the number of ice-free days over the southern Chukchi shelf between 2000 and 2012, a linear decrease in sea ice persistence has been observed over the northern Chukchi shelf and shelfbreak (Frey et al., 2015). The ^{228}Ra activities observed over the Chukchi shelf during our 2015 transect are similar to those measured on previous expeditions (Kipp, 2018); thus, changing shelf inputs are unlikely to bias our estimate of the ventilation time scale but should be considered in future studies in this region.

4.3. Recent Ventilation of the Makarov Basin

Arctic intermediate waters, which extend roughly from the halocline to the sill depth of the Lomonosov Ridge (~1,700 m), originate in the North Atlantic and are either transported into the Arctic through the Fram Strait or via the Barents Sea (e.g. Rudels et al., 1994, 2015, 2013; Schlosser et al., 1997; Smethie et al., 2000). The two Atlantic water masses meet following the subduction of the Barents Sea branch in the St. Anna Trough in the Kara Sea (Dmitrenko et al., 2015). Intermediate waters move cyclonically around the Arctic; one pathway follows the Eurasian side of the Lomonosov Ridge and another crosses the Lomonosov to enter the Makarov and Canada Basins (Rudels et al., 1994; Schauer et al., 1997; Smethie et al., 2000). Anthropogenically sourced tracers such as ^{3}H, SF_6, ^{129}I, and ^{236}U have been used to denote recent ventilation of intermediate water in the Amundsen, Canada, and Makarov Basins and indicate that the residence time of this water mass is on the order of decades (Casacuberta et al., 2018; Ekwurzel et al., 2001; Rutgers van der Loeff et al., 2018; Schlosser et al., 1999; Smethie et al., 2000; Smith et al., 2011; Smethie & Swift, 2018; Tanhua et al., 2009).

Elevated ^{228}Ra activities and ^{228}Ra/^{226}Ra activity ratios have also been used to identify recently ventilated waters as they move along isopycnals (Kim et al., 2003; Rutgers van der Loeff et al., 1995), and ^{228}Ra/^{226}Ra

activity ratios have been applied in the Arctic to determine the time elapsed since intermediate waters were last in contact with the shelf (Kadko & Aagaard, 2009; Rutgers van der Loeff et al., 2018). Radium-228 activities were elevated between 500 and 1,500 m on the northbound HLY1502 transect, coincident with increased oxygen and SF_6 concentrations (Landing et al., 2016; Smethie & Swift, 2018; Figures 3 and S8). If the shelf end-member is known, this signal of recent ventilation can be used to estimate the time elapsed since the water mass was ventilated using equation (1). In this case, $\left(\frac{^{228}Ra}{^{226}Ra}\right)_t$ is the activity ratio of $^{228}Ra/^{226}Ra$ observed in the intermediate water and $\left(\frac{^{228}Ra}{^{226}Ra}\right)_0$ is the ratio of the shelf end-member. The ratio of $^{228}Ra/^{226}Ra$ is used instead of the absolute ^{228}Ra activity in order to correct for any dilution or mixing during transit, assuming that the deep water has a negligible ^{228}Ra activity.

This approach assumes that there are no additional inputs of Ra from the slope after the water leaves the shelf. The $^{228}Ra/^{226}Ra$ activity ratios measured between 500 and 1,500 m at the HLY1502 stations closest to the slope (14, 57, 60) ranged from 0.02 to 0.09 (excluding one sample with a ratio of 0.58 ± 0.18 that is questionable due to a pump malfunction), indicating that inputs from the slope are unlikely to bias this calculation (Figures S6, S8, and S9). Elevated oxygen saturation and SF_6 concentrations between 500 and 1,500 m in the Makarov Basin also indicate recent ventilation (Smethie & Swift, 2018), and the atmospheric source of these tracers support recent contact with the shelf.

The $^{228}Ra/^{226}Ra$ activity ratios observed in the recently ventilated water at station 19 (above the Mendeleyev Ridge in the Canadian Basin) and station 32 (in the Amundsen Basin) were 0.15 ± 0.02 and 0.16 ± 0.01, respectively (Figures 3 and S9). Because this intermediate water was most recently in contact with the shelf during subduction through the St. Anna Trough in the Kara Sea (Rudels et al., 1994; Schauer et al., 1997), we use historical observations of the $^{228}Ra/^{226}Ra$ activity ratio from the Kara Sea as the shelf end-member. Using the average Kara Sea ratio of 2.1 ± 0.6 (Rutgers van der Loeff et al., 2003), the ventilation time scale is 18–25 years for the intermediate water at station 19 (above the Mendeleyev Ridge) and 18–24 years for the intermediate water at station 32 in the Amundsen Basin. Because similar mid-water column enrichments were not observed in the Canada Basin, the intermediate water in this basin must be ventilated on time scales greater than 30 years, after which time any ^{228}Ra enrichment would not be detectable. This is consistent with the current understanding of intermediate water circulation, which indicates that water flows through the Makarov Basin before reaching the Canada Basin (Rudels et al., 1994).

Rising shelf inputs of Ra as a result of climate change could bias this calculation toward older ages (Kipp et al., 2018; Rutgers van der Loeff et al., 2018), but because the Kara Sea measurements were made ~20 years before the HLY1502 transect, they are likely representative of end-member ratios at the time the intermediate water was subducted. Our intermediate water ventilation time scales also agree well with other recent estimates for the Amundsen, Makarov, and Canada Basins. Using SF_6 and CFC concentrations measured on the HLY1502 expedition, Smethie and Swift (2018) determined ventilation time scales of 15–24 years for intermediate waters (300–1,500 m) above the Mendeleyev Ridge and 27–42 years for intermediate waters in the Canada Basin. Amundsen Basin intermediate water ventilation times were estimated to be 15–27 years based on ^{228}Ra activities, SF_6 concentrations, and $^{129}I/^{236}U$ ratios measured on a concurrent European-led GEOTRACES expedition (PS94/GN04) that conducted more extensive sampling in this basin (Rutgers van der Loeff et al., 2018; Smethie & Swift, 2018).

These basin-specific constraints on intermediate water ventilation time scales provide important baselines against which future changes can be monitored. Climate change is causing shifts in freshwater storage that may affect brine formation: increased runoff may inhibit brine creation during periods of ice growth, but longer open water seasons allow storms to increase mixing and reduce stratification (McClelland et al., 2012). Additionally, the amplitude of the annual ice formation and melt cycle is increasing, and ice is being transported farther during its lifetime (Newton et al., 2017). Continued monitoring of ^{228}Ra activities in Arctic intermediate waters may help determine whether these freshwater changes will impact intermediate water formation and transport times.

4.4. Deep Water Residence Times

Radium-226 shows a positive correlation with Si, but the slope of the relationship varies with depth (Figures 7 and S12; Si concentrations from Kadko et al., 2016). Above the deep thermocline (~50–400 m),

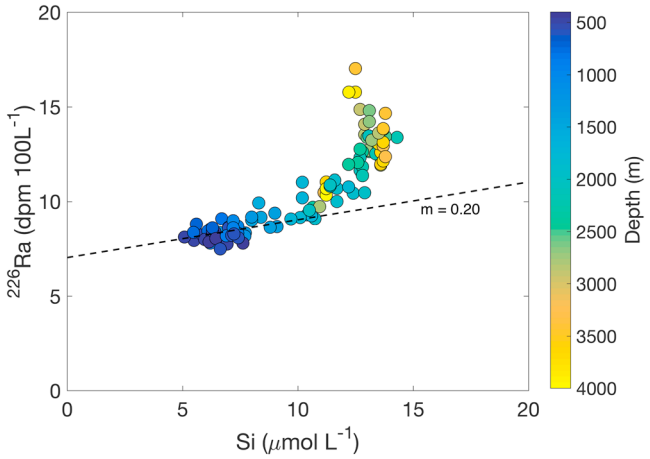

Figure 7. Radium-226 versus silica for samples collected below 400 m. Dashed line shows the ^{226}Ra-Si relationship between 400 and 1,500 m, which has a slope (m; units of 10^3 dpm/mol^{-1}) of 0.20 ± 0.11. This water enters the Arctic partly through the Fram Strait and partly through the Barents and Kara Seas (Rudels et al., 1994) such that the ^{226}Ra-Si relationship should be similar to that observed in the Greenland and Norwegian Seas. The ^{226}Ra-Si correlation observed in the Greenland Sea during the Transient Tracers in the Ocean (TTO) and GEOSECS programs was 0.20 ± 0.02 (Broecker et al., 1976; Key et al., 1992). Thus, the ^{226}Ra-Si relationship determined for the Arctic intermediate waters matches that of the source waters, and is not noticeably changed during transit over the Barents and Kara Seas. Below 1,500 m, the slope increases, reflecting an addition of ^{226}Ra without a corresponding increase in Si.

the slope of the ^{226}Ra-Si correlation (in units of 10^3 dpm/mol) is 0.15 ± 0.02 (Figure S12). In the cold Atlantic layer between 400 and 1,500 m, the slope of the ^{226}Ra-Si correlation is 0.20 ± 0.11 (Figure 7). Below 1,500 m, the slope of the ^{226}Ra-Si relationship increases significantly, indicating an addition of ^{226}Ra without an accompanying increase in Si (Figure 7). The ^{226}Ra-Ba relationships were similar to the ^{226}Ra-Si correlations (L. Whitmore, personal communications). The increase in ^{226}Ra without a concomitant increase in Ba or Si indicates that the increase is not due to sinking particle remineralization, which would also impact these other tracers, but rather to benthic sediment inputs of ^{226}Ra. Similar excess ^{226}Ra values have been observed in deep waters in other ocean basins (Broecker et al., 1976; Chung, 1980), and were first recorded in the Arctic over the Alpha Ridge in 1983 (Moore & Smith, 1986). Deviations from a linear ^{226}Ra-Ba relationship have also been recently documented in the Makarov Basin, but similar ^{226}Ra enrichments have not been observed in the Amundsen Basin (Rutgers van der Loeff et al., 2018). Our measurements of relatively low ^{226}Ra activities at station 32 in the Amundsen Basin are similar to the previously documented low ^{226}Ra activities in this region.

This accumulation of ^{226}Ra in the deep Canadian Basin can be used to estimate the residence time of deep waters. Radium-226 is constantly produced through the decay of ^{230}Th in sediments and is released into overlying bottom waters through diffusion, bioturbation, and sediment resuspension (Cochran & Krishnaswami, 1980). In the deep ocean, ^{226}Ra is removed from the water column through decay and mixing. To our knowledge, there are no hydrothermal vents in the Canadian Basin that could act as a source of ^{226}Ra to deep waters; although the Gakkel Ridge in the Eurasian Basin is hydrothermally active (Edmonds et al., 2003), it is unlikely that inputs from this ridge will be transported across the shallower Lomonosov Ridge. The balance between the addition of ^{226}Ra from sediments and the loss to decay and mixing can be used to estimate the residence time (τ_{res}) of the deep waters using the following equation (modified from Rutgers van der Loeff et al., 2018):

$$\tau_{res} = \frac{I}{F_{seds} - I \cdot \lambda_{226}} \quad (2)$$

where I is the difference between the observed ^{226}Ra inventory and that which is expected based on the ^{226}Ra-Si relationship of the source waters, λ_{226} is the decay constant of ^{226}Ra, and F_{seds} is the flux of ^{226}Ra from sediments. The expected ^{226}Ra activity was modeled based on the Si concentration at each depth where a ^{226}Ra sample was collected and the ^{226}Ra-Si relationship in the Atlantic layer (^{226}Ra = (0.20 ± 0.11) × Si + (7.0 ± 0.8)), and then the ^{226}Ra inventory was determined from the difference between this model curve and the observed ^{226}Ra profile below 1,500 m (above this depth the model agreed with observations).

The flux of ^{226}Ra across the sediment-water interface was estimated from the inventory of ^{230}Th in the sediment mixed layer. This inventory was converted to a flux of ^{226}Ra using the Cochran (1980) relationship, where the ^{226}Ra sediment flux varies as a function of the ^{230}Th inventory in the sediment mixed layer. The ^{230}Th inventory in sediments in the Makarov Basin was calculated from ^{230}Th profiles measured in cores collected on the AOS-94 expedition (Huh et al., 1997). To our knowledge only one sediment profile of ^{230}Th, collected from the T3 ice station (83.03°N, 163.57°W), exists for the Canada Basin (Ku & Broecker, 1965). Because of the limited data for this basin, we used the range in inventories observed in cores from both basins to estimate the ^{230}Th inventory for Canada Basin sediments; we expect the ^{230}Th inventories in Makarov and Canada Basin sediments to be similar because ^{230}Th deposition in sediments depends in part on water column depth (Bacon & Anderson, 1982) and the bottom depths of the two basins are comparable. Using supported ^{210}Pb activities in these AOS-94 cores as a proxy for ^{226}Ra activities, ^{226}Ra reaches

equilibrium with ^{230}Th approximately 5 cm below the sediment-water interface (at ~10 dpm/g; Huh et al., 1997). The ^{226}Ra/^{230}Th activity ratios reported for the T3 sediment core also indicate that equilibrium is reached between 5 and 10 cm (Ku & Broecker, 1965). Above this depth, it is assumed that ^{226}Ra produced through decay of ^{230}Th can be lost via diffusion into the overlying water column; thus, ^{230}Th inventories were integrated down to 5 cm in order to estimate the flux of ^{226}Ra across the sediment-water interface. The ^{230}Th inventories in the top 5 cm of the three cores available from the Makarov Basin were 60–70 dpm/cm^2. These inventories correspond to estimated ^{226}Ra fluxes of ~0.02–0.03 dpm·cm^{-2}·yr^{-1} (Cochran, 1980). The ^{230}Th inventory in the top 5 cm of the T3 core from the Canada Basin was 90 dpm/cm^2, which corresponds to a ^{226}Ra flux of ~0.035 dpm·cm^{-2}·yr^{-1} (Cochran, 1980). These values are well within the range of estimates for other ocean basins (0.002–0.2 dpm·cm^{-2}·yr^{-1}; Cochran, 1980). Based on the observed deficit of ^{226}Ra with respect to ^{230}Th in a core collected on the Mendeleyev Ridge, Not et al. (2008) estimated a slightly higher ^{226}Ra flux of 0.043 dpm·cm^{-2}·yr^{-1}. A larger flux would serve to decrease the residence time estimates.

The residence time of deep water in the Makarov Basin was determined to be 400–650 years based on the ^{226}Ra profile at station 30 (Figure S10) and the range in the ^{226}Ra flux from sediments in the Makarov Basin. This value is similar to previous estimates of ~300–600 years (Jones et al., 1995; Schlosser et al., 1997; Tanhua et al., 2009; Casacuberta et al., 2018; Rutgers van der Loeff et al., 2018). The deep waters at stations 48, 52, and 57 in the deep Canada Basin (Figure S10) were determined to have residence times of 130–270 years based on the range of ^{226}Ra fluxes estimated for sediments in both the Makarov and Canada Basins. These residence times are shorter than previous estimates of ~230–500 years (Deng et al., 2018; Macdonald et al., 1993; Schlosser et al., 1997; Tanhua et al., 2009). However, this calculation is very sensitive to the ^{230}Th inventory, and integrating the AOS-94 cores to 3 cm, the maximum mixed layer thickness (Clough et al., 1997; Smith et al., 2003), instead of 5 cm, yields a ^{230}Th inventory of 40–50 dpm/cm^2. This correlates to a ^{226}Ra flux of ~0.01–0.015 dpm·cm^{-2}·yr^{-1} and a residence time of 330–610 years, which is in better agreement with previous estimates. Due to the large uncertainties associated with the ^{226}Ra flux from sediments, these residence time estimates should be refined with more measurements of ^{230}Th and ^{226}Ra in Arctic basin sediments, particularly those collected from the central Canada Basin.

5. Conclusions

We measured radium isotopes in the Western Arctic from the Chukchi Shelf to the North Pole on the 2015 HLY1502 transect, and applied this extensive data set to examine shelf inputs, time scales of halocline ventilation, and deep water residence times in the Western Arctic Ocean. By combining our 2015 data with Ra measurements made in the Chukchi Sea and southern Canada Basin in the late 1990s and 2000s, we have identified persistent shelf signals in surface waters and the halocline. Strong shelf influence was identified in the Transpolar Drift and at the Chukchi shelfbreak, and the time scale of halocline ventilation with respect to inputs from the Chukchi shelf was estimated to be $\leq$19–23 years.

Radium-228 enrichments in intermediate waters above the Mendeleyev Ridge and in the Amundsen Basin suggest recent communication with shelf waters; ^{228}Ra/^{226}Ra activity ratios were used to determine ventilation time scales of 18–25 years for these water masses. The lack of a similar ^{228}Ra enrichment in the Canada Basin indicates that intermediate water in this basin has been isolated from the shelf for at least 30 years. Radium-226 activities were high in the deep Makarov and Canada Basins, and, due to sediment input, deviated from the intermediate water ^{226}Ra-Si relationship. Based on these ^{226}Ra enrichments, the residence time of deep waters in the Makarov and Canada Basins were estimated to be 400–650 and 130–270 years, respectively. These estimates can be refined with more measurements of ^{226}Ra and ^{230}Th in sediments in the Canadian Basin.

Changes in the Arctic climate are likely to affect shelf-basin interactions and freshwater storage in this basin. This data set provides important baseline observations and residence time estimates for intermediate and deep waters in the Western Arctic. Continued monitoring of radium isotopes in the Arctic could help track changes brought about by rising air and sea temperatures in this region. Specifically, changes in shelf-derived material inputs may increase as ice cover decreases over shelves, which would allow greater water column mixing; with its shelf source and low biological and particle reactivity, ^{228}Ra can be used to trace

these changes in sediment flux to the open ocean. The ventilation time scales provided by $^{228}Ra/^{226}Ra$ activity ratios can also be used to monitor whether changes in brine formation over the shelves impact the residence time of intermediate waters. Future studies should focus on constraining seasonal variability, and on providing Ra measurements from the currently undersampled Eastern Chukchi and East Siberian Seas.

Acknowledgments
We thank the captain and crew of the *USCGC Healy* (HLY1502) and the chief scientists D. Kadko and W. Landing for coordinating a safe and successful expedition. We thank the members of the pump team, P. Lam, E. Black, S. Pike, X. Yang, and M. Heller for their assistance with sample collection and for their unfailingly positive attitudes during this 65-day expedition. We also appreciate sampling assistance from P. Aguilar and M. Stephens, and MATLAB assistance from B. Corlett, A. Pacini, P. Lin, and M. Li. The radium data from the HLY1502 expedition are available through the Biological & Chemical Oceanography Data Management Office (https://www.bco-dmo.org/dataset/718440) and the radium measurements from the SHEBA, AWS-2000, and SBI expeditions can be found in the supporting information. This work was funded by NSF awards OCE-1458305 to M.A.C., OCE-1458424 to W. S.M., and PLR-1504333 to R.S.P. This research was conducted with Government support under and awarded by a DoD, Air Force Office of Scientific Research, National Defense Science and Engineering Graduate (NDSEG) Fellowship awarded to L.E. K., 32 CFR 168a.

References

Aagaard, K., & Carmack, E. C. (1989). The role of sea ice and other fresh water in the Arctic circulation. *J. Geophys. Res.*, *94*, 14,485–14,498.

Aagaard, K., Coachman, L. K., & Carmack, E. (1981). On the halocline of the Arctic Ocean. *Deep Sea Research Part A. Oceanographic Research Papers*, *28*(6), 529–545. https://doi.org/10.1016/0198-0149(81)90115-1

Amiel, D., & Cochran, J. K. (2008). Terrestrial and marine POC fluxes derived from ^{234}Th distributions and $\delta^{13}C$ measurements on the Mackenzie Shelf. *Journal of Geophysical Research*, *113*, C03S06. https://doi.org/10.1029/2007JC004260

Arrigo, K. R., Mills, M. M., van Dijken, G. L., Lowry, K. E., Pickart, R. S., & Schlitzer, R. (2017). Late spring nitrate distributions beneath the ice-covered northeastern Chukchi Shelf. *Journal of Geophysical Research: Biogeosciences*, *122*, 2409–2417. https://doi.org/10.1002/2017JG003881

Bacon, M. P., & Anderson, R. F. (1982). Distribution of thorium isotopes between dissolved and particulate forms in the deep sea. *Journal of Geophysical Research*, *87*, 2045–2056. https://doi.org/10.1029/JC087iC03p02045

Black, E. E. (2017). An investigation of basin-scale controls on upper ocean export and remineralization, doctoral dissertation. Massachusetts Institute of Technology, Woods Hole Oceanographic Institution. URL: http://hdl.handle.net/1721.1/115781

Broecker, W. S., Goddard, J., & Sarmiento, J. L. (1976). The distribution of ^{226}Ra in the Atlantic Ocean. *Earth and Planetary Science Letters*, *32*(2), 220–235. https://doi.org/10.1016/0012-821X(76)90063-7

Cai, W.-J., Hu, X., Huang, W.-J., Jiang, L.-Q., Wang, Y., Peng, T.-H., & Zhang, X. (2010). Alkalinity distribution in the western North Atlantic Ocean margins. *Journal of Geophysical Research*, *115*, C08014. https://doi.org/10.1029/2009JC005482

Carmack, E., & Chapman, D. C. (2003). Wind-driven shelf/basin exchange on an Arctic shelf: The joint roles of ice cover extent and shelf-break bathymetry. *Geophysical Research Letters*, *30*(14), 1778. https://doi.org/10.1029/2003GL017526

Carmack, E., & Wassmann, P. (2006). Food webs and physical-biological coupling on pan-Arctic shelves: Unifying concepts and comprehensive perspectives. *Progress in Oceanography*, *71*, 446–477. https://doi.org/10.1016/j.pocean.2006.10.004

Carmack, E. C., Yamamoto-Kawai, M., Haine, T. W. N., Bacon, S., Bluhm, B. A., Lique, C., et al. (2016). Freshwater and its role in the Arctic Marine System: Sources, disposition, storage, export, and physical and biogeochemical consequences in the Arctic and global oceans. *Journal of Geophysical Research: Biogeosciences*, *121*, 675–717. https://doi.org/10.1002/2015JG003140

Casacuberta, N., Christl, M., Vockenhuber, C., Wefing, A. M., Wacker, L., Masqué, P., et al. (2018). Tracing the three atlantic branches entering the Arctic Ocean with ^{129}I and ^{236}U. *Journal of Geophysical Research: Oceans*, *123*, 6909–6921. https://doi.org/10.1029/2018JC014168

Chan, L. H., Edmond, J. M., Stallard, R. F., Broecker, W. S., Chung, Y. C., Weiss, R. F., & Ku, T. L. (1976). Radium and barium at GEOSECS stations in the Atlantic and Pacific. *Earth and Planetary Science Letters*, *32*(2), 258–267. https://doi.org/10.1016/0012-821X(76)90066-2

Charette, M. A., Dulaiova, H., Gonneea, M. E., Henderson, P. B., Moore, W. S., Scholten, J. C., & Pham, M. K. (2012). GEOTRACES radium isotopes interlaboratory comparison experiment. *Limnology and Oceanography: Methods*, *10*(6), 451–463. https://doi.org/10.4319/lom.2012.10.451

Charette, M. A., Morris, P. J., Henderson, P. B., & Moore, W. S. (2015). Radium isotope distributions during the US GEOTRACES North Atlantic cruises. *Marine. Chemistry*, *177*, 184–195. https://doi.org/10.1016/j.marchem.2015.01.001

Chung, Y. (1980). Radium-barium-silica correlations and a two-dimensional radium model for the world ocean. *Earth and Planetary Science Letters*, *49*(2), 309–318. https://doi.org/10.1016/0012-821X(80)90074-6

Chung, Y., & Craig, H. (1980). ^{226}Ra in the Pacific Ocean. *Earth and Planetary Science Letters*, *49*(2), 267–292. https://doi.org/10.1016/0012-821X(80)90072-2

Clough, L. M., Jr, W. G. A., Cochran, K., Barnes, K., Renaud, P. P., & Aller, R. (1997). Bioturbation, biomass, and infaunal abundance in the sediments of the Arctic Ocean. *Deep Sea Research Part II: Topical Studies in Oceanography*, *44*(8), 1683–1704. https://doi.org/10.1016/S0967-0645(97)00052-0

Cochran, J. K. (1980). The flux of ^{226}Ra from deep-sea sediments. *Earth and Planetary Science Letters*, *49*(2), 381–392. https://doi.org/10.1016/0012-821X(80)90080-1

Cochran, J. K., & Krishnaswami, S. (1980). Radium, thorium, uranium, and ^{210}Pb in deep-sea sediments and sediment pore waters from the North Equatorial Pacific. *American Journal of Science*, *280*, 849–889.

Corlett, W. B., & Pickart, R. S. (2017). The Chukchi slope current. *Progress in Oceanography*, *153*, 50–65. https://doi.org/10.1016/j.pocean.2017.04.005

Deng, H., Ke, H., Huang, P., Chen, X., & Cai, M. (2018). Ventilation time and anthropogenic CO_2 in the Bering Sea and the Arctic Ocean based on carbon tetrachloride measurements. *Journal of Oceanography*, *74*(5), 439–452. https://doi.org/10.1007/s10872-018-0471-3

Dmitrenko, I. A., Rudels, B., Kirillov, S. A., Aksenov, Y. O., Lien, V. S., Ivanov, V. V., et al. (2015). Atlantic water flow into the Arctic Ocean through the St. Anna Trough in the northern Kara Sea. *Journal of Geophysical Research: Oceans*, *120*, 5158–5178. https://doi.org/10.1002/2015JC010804

Edmonds, H. N., Michael, P. J., Baker, E. T., Connelly, D. P., Snow, J. E., Langmuir, C. H., et al. (2003). Discovery of abundant hydrothermal venting on the ultraslow-spreading Gakkel ridge in the Arctic Ocean. *Nature*, *421*(6920), 252–256. https://doi.org/10.1038/nature01351

Ekwurzel, B., Schlosser, P., Mortlock, R. A., Fairbanks, R. G., & Swift, J. H. (2001). River runoff, sea ice meltwater, and Pacific water distribution and mean residence times in the Arctic Ocean. *Journal of Geophysical Research*, *106*(C5), 9075–9092. https://doi.org/10.1029/1999JC000024

Frey, K. E., Moore, G. W. K., Cooper, L. W., & Grebmeier, J. M. (2015). Divergent patterns of recent sea ice cover across the Bering, Chukchi, and Beaufort Seas of the Pacific Arctic Region. *Progress in Oceanography*, *136*, 32–49. https://doi.org/10.1016/j.pocean.2015.05.009

Gong, D., & Pickart, R. S. (2016). Early summer water mass transformation in the eastern Chukchi Sea. *Deep Sea Research Part II: Topical Studies in Oceanography*, *130*, 43–55. https://doi.org/10.1016/j.dsr2.2016.04.015

Günther, F., Overduin, P. P., Sandakov, A. V., Grosse, G., & Grigoriev, M. N. (2013). Short- and long-term thermo-erosion of ice-rich permafrost coasts in the Laptev Sea region. *Biogeosciences*, *10*(6), 4297–4318. https://doi.org/10.5194/bg-10-4297-2013

Hansell, D. A., Kadko, D., & Bates, N. R. (2004). Degradation of terrigenous dissolved organic carbon in the Western Arctic Ocean. *Science*, *304*(5672), 858–861. https://doi.org/10.1126/science.1096175

Henderson, P. B., Morris, P. J., Moore, W. S., & Charette, M. A. (2013). Methodological advances for measuring low-level radium isotopes in seawater. *Journal of Radioanalytical and Nuclear Chemistry*, *296*, 357–362. https://doi.org/10.1007/s10967-012-2047-9

Huh, C. A., Pisias, N. G., Kelley, J. M., Maiti, T. C., & Grantz, A. (1997). Natural radionuclides and plutonium in sediments from the western Arctic Ocean: Sedimentation rates and pathways of radionuclides. *Deep Sea Research Part II: Topical Studies in Oceanography*, *44*(8), 1725–1743. https://doi.org/10.1016/S0967-0645(97)00040-4

Jakobsson, M. (2002). Hypsometry and volume of the Arctic Ocean and its constituent seas. *Geochemistry, Geophysics, Geosystems*, *3*(5), 1028. https://doi.org/10.1029/2001GC000302

Jones, E. P., Rudels, B., & Anderson, L. G. (1995). Deep waters of the Arctic Ocean: Origins and circulation. *Deep Sea Research Part I: Oceanographic Research Papers*, *42*(5), 737–760. https://doi.org/10.1016/0967-0637(95)00013-V

Kadko, D., & Aagaard, K. (2009). Glimpses of Arctic Ocean shelf–basin interaction from submarine-borne radium sampling. *Deep Sea Research Part I: Oceanographic Research Papers*, *56*, 32–40. https://doi.org/10.1016/j.dsr.2008.08.002

Kadko, D., Landing, W. M., & Cutter, G. A. (2016). CTD-ODF bottles from GEOTRACES-Arctic Section cruise HLY1502. Biological and Chemical Oceanography Data Management Office (BCO-DMO). Dataset version 2016-09-01, Available from: http://lod.bco-dmo.org/id/dataset/646825

Kadko, D., & Muench, R. (2005). Evaluation of shelf-basin interaction in the western Arctic by use of short-lived radium isotopes: The importance of mesoscale processes. *Deep Sea Research Part I: Oceanographic Research Papers*, *52*(24–26), 3227–3244. https://doi.org/10.1016/j.dsr2.2005.10.008

Kadko, D., Pickart, R. S., & Mathis, J. (2008). Age characteristics of a shelf-break eddy in the western Arctic and implications for shelf-basin exchange. *Journal of Geophysical Research*, *113*, C02018. https://doi.org/10.1029/2007JC004429

Kaufman, A., Trier, R. M., Broecker, W. S., & Feely, H. W. (1973). Distribution of ^{228}Ra in the world ocean. *Journal of Geophysical Research*, *78*(36), 8827–8848. https://doi.org/10.1029/JC078i036p08827

Key, R. M., Brewer, R. L., Stockwell, J. H., Guinasso, N. L., & Schink, D. R. (1979). Some improved techniques for measuring radon and radium in marine sediments and in seawater. *Marine Chemistry*, *7*(3), 251–264. https://doi.org/10.1016/0304-4203(79)90042-2

Key, R. M., Moore, W. S., & Sarmiento, J. L. (1992). Transient tracers in the ocean north Atlantic study final data report for ^{228}Ra and ^{226}Ra. Technical Report *#92-2*, Princeton.

Kim, G., Hussain, N., & Church, T. M. (2003). Tracing the advection of organic carbon into the subsurface Sargasso Sea using a ^{228}Ra/^{226}Ra tracer. *Geophysical Research Letters*, *30*(16), 1874. https://doi.org/10.1029/2003GL017565

Kipp, L. (2018). Radium isotopes as tracers of boundary inputs of nutrients and trace elements to the coastal and open ocean, doctoral dissertation. Massachusetts Institute of Technology and Woods Hole Oceanographic Institution. URL: http://hdl.handle.net/1721.1/119990

Kipp, L. E., Charette, M. A., Moore, W. S., Henderson, P. B., & Rigor, I. G. (2018). Increased fluxes of shelf-derived materials to the central Arctic Ocean. *Science Advances*, *4*(1). https://doi.org/10.1126/sciadv.aao1302

Ku, T.-L., & Broecker, W. S. (1965). Rates of sedimentation in the Arctic ocean. *Progress in Oceanography*, *4*(964), 95–104. https://doi.org/10.1016/0079-6611(65)90043-1

Landing, W. M., Cutter, G. A., & Kadko, D. C. (2016). CTD-GTC profiles from GEOTRACES-Arctic Section cruise HLY1502 in 2015 (U.S. GEOTRACES Arctic project). Biological and Chemical Oceanography Data Management Office (BCO-DMO). Dataset version 2016-07-12, Retrieved from https://www.bco-dmo.org/dataset/651599

Li, M., Pickart, R. S., Spall, M. A., Weingartner, T. J., Lin, P., Moore, G. W. K., & Qi, Y. (2019). Circulation of the Chukchi Sea shelfbreak and slope from moored timeseries. *Progress in Oceanography*. https://doi.org/10.1016/j.pocean.2019.01.002

Lowry, K. E., Pickart, R. S., Mills, M. M., Brown, Z. W., van Dijken, G. L., Bates, N. R., & Arrigo, K. R. (2015). The influence of winter water on phytoplankton blooms in the Chukchi Sea. *Deep Sea Research Part II: Topical Studies in Oceanography*, *118*, 53–72. https://doi.org/10.1016/j.dsr2.2015.06.006

Luo, D., Wu, Q., Jin, H., Marchenko, S. S., Lü, L., & Gao, S. (2016). Recent changes in the active layer thickness across the northern hemisphere. *Environmental Earth Sciences*, *75*(7). https://doi.org/10.1007/s12665-015-5229-2

Ma, Q., Chen, M., Qiu, Y., & Li, Y. (2005). Regional estimates of POC export flux derived from thorium-234 in the western Arctic Ocean. *Acta Oceanologica Sinica*, *24*(6), 97–108.

Macdonald, R. W., Carmack, E. C., & Wallace, D. W. R. (1993). Tritium and radiocarbon dating of Canada Basin deep waters. *Science*, *259*(5091), 103–104. https://doi.org/10.1126/science.259.5091.103

Maiti, K., Charette, M. A., Buesseler, K. O., Zhou, K., Henderson, P., Moore, W. S., et al. (2015). Determination of particulate and dissolved ^{228}Th in seawater using a delayed coincidence counter. *Marine Chemistry*, *177*, 196–202. https://doi.org/10.1016/j.marchem.2014.12.001.

Mathis, J. T., Pickart, R. S., Hansell, D. A., Kadko, D., & Bates, N. R. (2007). Eddy transport of organic carbon and nutrients from the Chukchi Shelf: Impact on the upper halocline of the western Arctic Ocean. *Journal of Geophysical Research*, *112*, C05011. https://doi.org/10.1029/2006JC003899

McClelland, J. W., Holmes, R. M., Dunton, K. H., & Macdonald, R. W. (2012). The Arctic ocean estuary. *Estuaries and Coasts*, *35*(2), 353–368. https://doi.org/10.1007/s12237-010-9357-3

Moore, M., & Smith, N. (1986). Disequilibria between ^{226}Ra, ^{210}Pb and ^{210}Po in the Arctic Ocean and the implications for chemical modification of the Pacific water inflow. *Earth and Planetary Science Letters*, *77*, 285–292.

Moore, W. S. (2000a). Ages of continental shelf waters determined from ^{223}Ra and ^{224}Ra. *Journal of Geophysical Research*, *105*(C9), 22,117–22,122. https://doi.org/10.1029/1999JC000289

Moore, W. S. (2000b). Determining coastal mixing rates using radium isotopes. *Continental Shelf Research*, *20*(1), 993–2007. https://doi.org/10.1016/S0278-4343(00)00054-6

Moore, W. S., & Arnold, R. (1996). Measurement of ^{223}Ra and ^{224}Ra in coastal waters using a delayed coincidence counter. *Journal of Geophysical Research*, *101*, 1321–1329. https://doi.org/10.1029/95JC03139

Muench, R. D., Gunn, J. T., Whitledge, T. E., Schlosser, P., & Smethie, W. (2000). An Arctic Ocean cold core eddy. *Journal of Geophysical Research*, *105*, 23,997. https://doi.org/10.1029/2000JC000212

Muench, R. D., Schumacher, J. D., & Salo, S. A. (1988). Winter currents and hydrographic conditions on the northern central Bering Sea shelf. *Journal of Geophysical Research*, *93*(C1), 516–526. https://doi.org/10.1029/JC093iC01p00516

Newton, R., Pfirman, S., Tremblay, B., & DeRepentigny, P. (2017). Increasing transnational sea-ice exchange in a changing Arctic Ocean. *Earth's Future*, *5*, 633–647. https://doi.org/10.1002/2016EF000500

Not, C., Hillaire-Marcel, C., Ghaleb, B., Polyak, L., & Darby, D. (2008). ^{210}Pb–^{226}Ra–^{230}Th systematics in very low sedimentation rate sediments from the Mendeleev Ridge (Arctic Ocean), edited by P. Hollings. *Canadian Journal of Earth Sciences*, *45*(11), 1207–1219. https://doi.org/10.1139/E08-047

Östlund, H. G. (1982). The residence time of the freshwater component in the Arctic Ocean. *Journal of Geophysical Research*, *87*(C3), 2035. https://doi.org/10.1029/JC087iC03p02035

Östlund, H. G., & Hut, G. (1984). Arctic Ocean water mass balance from isotope data. *Journal of Geophysical Research*, *89*(C4), 6373. https://doi.org/10.1029/JC089iC04p06373

Pacini, A., Pickart, R. S., Moore, G. W. K., & Våge, K. (2016). Hydrographic structure and modification of Pacific winter water on the Chukchi Sea shelf in late spring. Abstract H14B-1406 in Ocean Sciences Meeting, New Orleans, Louisiana, USA.

Paquette, R. G., & Bourke, R. H. (1974). Observations on the coastal current of Arctic Alaska. *Journal of Marine Research*, *32*(2), 195–207.

Pasqualini, A., Schlosser, P., Newton, R., & Koffman, T. N. (2017). U.S. GEOTRACES Arctic Section Ocean Water Hydrogen and Oxygen Stable Isotope Analyses. *Interdisciplinary Earth Data Alliance (IEDA)*. https://doi.org/10.1594/ieda/100633

Peterson, B. J., Holmes, R. M., McClelland, J. W., Vörösmarty, C. J., Lammers, R. B., Shiklomanov, A. I., et al. (2002). Increasing river discharge to the Arctic Ocean. *Science*, *298*(5601), 2171–2173. https://doi.org/10.1126/science.1077445

Pickart, R. S., Moore, G. W. K., Mao, C., Bahr, F., Nobre, C., & Weingartner, T. J. (2016). Circulation of winter water on the Chukchi shelf in early Summer. *Deep Sea Research Part II: Topical Studies in Oceanography*, *130*, 56–75. https://doi.org/10.1016/j.dsr2.2016.05.001

Pickart, R. S., Pratt, L. J., Torres, D. J., Whitledge, T. E., Proshutinsky, A. Y., Aagaard, K., et al. (2010). Evolution and dynamics of the flow through Herald Canyon in the western Chukchi Sea. *Deep Sea Research Part II: Topical Studies in Oceanography*, *57*(1–2), 5–26. https://doi.org/10.1016/j.dsr2.2009.08.002

Pickart, R. S., Weingartner, T. J., Pratt, L. J., Zimmermann, S., & Torres, D. J. (2005). Flow of winter-transformed Pacific water into the Western Arctic. *Deep Sea Research Part II: Topical Studies in Oceanography*, *52*(24–26), 3175–3198. https://doi.org/10.1016/j.dsr2.2005.10.009

Pisareva, M. N., Pickart, R. S., Spall, M. A., Nobre, C., Torres, D. J., Moore, G. W. K., & Whitledge, T. E. (2015). Flow of pacific water in the western Chukchi Sea: Results from the 2009 RUSALCA expedition. *Deep Sea Research Part I: Oceanographic Research Papers*, *105*, 53–73. https://doi.org/10.1016/j.dsr.2015.08.011

Rainville, L., & Woodgate, R. A. (2009). Observations of internal wave generation in the seasonally ice-free Arctic. *Geophysical Research Letters*, *36*, L23604. https://doi.org/10.1029/2009GL041291

Rawlins, M. A., Steele, M., Holland, M. M., Adam, J. C., Cherry, J. E., Francis, J. A., et al. (2010). Analysis of the Arctic system for freshwater cycle intensification: Observations and expectations. *Journal of Climate*, *23*(21), 5715–5737. https://doi.org/10.1175/2010JCLI3421.1

Rudels, B., Jones, E. P., Anderson, L. G., & Kattner, G. (1994). On the intermediate depth waters of the Arctic Ocean. In O. M. Johannessen, R. D. Muench, & J. E. Overland (Eds.), *The Polar Oceans and Their Role in Shaping the Global Environment* (pp. 33–46). Washington, DC: American Geophysical Union.

Rudels, B., Korhonen, M., Schauer, U., Pisarev, S., Rabe, B., & Wisotzki, A. (2015). Circulation and transformation of Atlantic water in the Eurasian Basin and the contribution of the Fram Strait inflow branch to the Arctic Ocean heat budget. *Progress in Oceanography*, *132*, 128–152. https://doi.org/10.1016/j.pocean.2014.04.003

Rudels, B., Schauer, U., Björk, G., Korhonen, M., Pisarev, S., Rabe, B., & Wisotzki, A. (2013). Observations of water masses and circulation with focus on the Eurasian Basin of the Arctic Ocean from the 1990s to the late 2000s. *Ocean Science*, *9*(1), 147–169. https://doi.org/10.5194/os-9-147-2013

Rutgers van der Loeff, M., Cai, P., Stimac, I., Bauch, D., Hanfland, C., Roeske, T., & Moran, S. B. (2012). Shelf-basin exchange times of Arctic surface waters estimated from ^{228}Th/^{228}Ra disequilibrium. *Journal of Geophysical Research*, *117*, C03024. https://doi.org/10.1029/2011JC007478

Rutgers van der Loeff, M., Key, R. M., Scholten, J., Bauch, D., & Michel, A. (1995). ^{228}Ra as a tracer for shelf water in the Arctic Ocean. *Deep Sea Research Part II: Topical Studies in Oceanography*, *42*(6), 1533–1553.

Rutgers van der Loeff, M., Kipp, L., Charette, M. A., Moore, W. S., Black, E., Stimac, I., et al. (2018). Radium isotopes across the Arctic Ocean show time scales of water mass ventilation and increasing shelf inputs. *Journal of Geophysical Research: Oceans*, *123*, 4853–4873. https://doi.org/10.1029/2018JC013888

Rutgers van der Loeff, M., Kuhne, S., Wahsner, M., Holtzen, H., Frank, M., Ekwurzel, B., et al. (2003). ^{228}Ra and ^{226}Ra in the Kara and Laptev seas. *Continental Shelf Research*, *23*, 113–124. https://doi.org/10.1016/S0304-4203(98)00070-X

Sanial, V., Kipp, L. E., Henderson, P. B., van Beek, P., Reyss, J. L., Hammond, D. E., et al. (2018). Radium-228 as a tracer of dissolved trace element inputs from the Peruvian continental margin. *Marine Chemistry*, *201*, 20–34. https://doi.org/10.1016/j.marchem.2017.05.008

Schauer, U., Muench, R. D., Rudels, B., & Timokhov, L. (1997). Impact of eastern Arctic shelf waters on the Nansen Basin intermediate layers. *Journal of Geophysical Research*, *102*(C2), 3371–3382. https://doi.org/10.1029/96JC03366

Schlosser, P., Bayer, R., Bönisch, G., Cooper, L. W., Ekwurzel, B., Jenkins, W. J., et al. (1999). Pathways and mean residence times of dissolved pollutants in the ocean derived from transient tracers and stable isotopes. *Science of the Total Environment*, *237–238*, 15–30. https://doi.org/10.1016/S0048-9697(99)00121-7

Schlosser, P., Kromer, B., Ekwurzel, B., Bönisch, G., McNichol, A., Schneider, R., et al. (1997). The first trans-Arctic ^{14}C section: Comparison of the mean ages of the deep waters in the Eurasian and Canadian basins of the Arctic Ocean. *Nuclear Instruments and Methods in Physics Research Section B: Beam Interactions with Materials and Atoms*, *123*, 431–437. https://doi.org/10.1016/S0168-583X(96)00677-5

Shimada, K., Carmack, E. C., Hatakeyama, K., & Takizawa, T. (2001). Varieties of shallow temperature maximum waters in the Western Canadian Basin of the Arctic Ocean. *Geophysical Research Letters*, *28*(18), 3441–3444. https://doi.org/10.1029/2001GL013168

Smethie, W. M., Schlosser, P., Bönisch, G., & Hopkins, T. S. (2000). Renewal and circulation of intermediate waters in the Canadian Basin observed on the SCICEX 96 cruise. *Journal of Geophysical Research*, *105*(C1), 1105–1121. https://doi.org/10.1029/1999JC900233

Smethie, W. M., & Swift, J. H. (2018). Distribution of CFCs and SF_6 measured on the 2015 GEOTRACES and repeat hydrography cruises to the Arctic Ocean, in Ocean Sciences Meeting, Portland, OR, USA.

Smith, J. N., McLaughlin, F. A., Smethie, W. M., Moran, S. B., & Lepore, K. (2011). Iodine-129, ^{137}Cs, and CFC-11 tracer transit time distributions in the Arctic Ocean. *Journal of Geophysical Research*, *116*, C04024. https://doi.org/10.1029/2010JC006471

Smith, J. N., Moran, S. B., & Macdonald, R. W. (2003). Shelf–basin interactions in the Arctic Ocean based on ^{210}Pb and Ra isotope tracer distributions. *Deep Sea Research Part I: Oceanographic Research Papers*, *50*, 397–416. https://doi.org/10.1016/S0967-0637(02)00166-8

Spall, M. A. (2007). Circulation and water mass transformation in a model of the Chukchi Sea. *Journal of Geophysical Research*, *112*, C05025. https://doi.org/10.1029/2005JC003364

Spall, M. A., Pickart, R. S., Fratantoni, P. S., & Plueddemann, A. J. (2008). Western Arctic shelfbreak eddies: Formation and transport. *Journal of Physical Oceanography*, *38*(8), 1644–1668. https://doi.org/10.1175/2007JPO3829.1

Spall, M. A., Pickart, R. S., Li, M., Itoh, M., Lin, P., Kikuchi, T., & Qi, Y. (2018). Transport of Pacific water into the Canada Basin and the formation of the Chukchi slope current. *Journal of Geophysical Research: Oceans*, *123*, 7453–7471. https://doi.org/10.1029/2018JC013825

Swift, J. H., Kadko, D. C., Smethie, W. M., Becker, S. M., Barna, A., Cummiskey, J., et al. (2016). The Arctic Ocean then and now: Preliminary hydrographic data from the 2015 US GEOTRACES Arctic expedition, in Ocean Sciences Meeting, New Orleans, Louisiana, USA.

Tanhua, T., Jones, E. P., Jeansson, E., Jutterström, S., Smethie, W. M., Wallace, D. W. R., & Anderson, L. G. (2009). Ventilation of the arctic ocean: Mean ages and inventories of anthropogenic CO_2 and CFC-11. *Journal of Geophysical Research*, *114*, C01002. https://doi.org/10.1029/2008JC004868

Timmermans, M.-L., Toole, J., Proshutinsky, A., Krishfield, R., & Plueddemann, A. (2008). Eddies in the Canada Basin, Arctic Ocean, observed from ice-tethered profilers. *Journal of Physical Oceanography*, *38*(1), 133–145. https://doi.org/10.1175/2007JPO3782.1

Vieira, L. H., Achterberg, E. P., Scholten, J., Beck, A. J., Liebetrau, V., Mills, M. M., & Arrigo, K. R. (2018). Benthic fluxes of trace metals in the Chukchi Sea and their transport into the Arctic Ocean. *Marine Chemistry*, *208*, 43–55. https://doi.org/10.1016/j.marchem.2018.11.001

Walvoord, M. A., Voss, C. I., & Wellman, T. P. (2012). Influence of permafrost distribution on groundwater flow in the context of climate-driven permafrost thaw: Example from Yukon Flats Basin, Alaska, United States. *Water Resources Research*, *48*, W07524. https://doi.org/10.1029/2011WR011595

Weingartner, T., Aagaard, K., Woodgate, R., Danielson, S., Sasaki, Y., & Cavalieri, D. (2005). Circulation on the north central Chukchi Sea shelf. *Deep Sea Research Part II: Topical Studies in Oceanography*, *52*(24–26), 3150–3174. https://doi.org/10.1016/j.dsr2.2005.10.015

Weingartner, T. J., Cavalieri, D. J., Aagaard, K., & Sasaki, Y. (1998). Circulation, dense water formation, and outflow on the northeast Chukchi Shelf. *Journal of Geophysical Research*, *103*(C4), 7647–7661. https://doi.org/10.1029/98JC00374

Weiss, R. F. (1970). The solubility of nitrogen, oxygen and argon in water and seawater. *Deep Sea Research Part II: Topical Studies in Oceanography*, *17*(4), 721–735. https://doi.org/10.1016/0011-7471(70)90037-9

Williams, W. J., & Carmack, E. C. (2015). The "interior" shelves of the Arctic Ocean: Physical oceanographic setting, climatology and effects of sea-ice retreat on cross-shelf exchange. *Progress in Oceanography*, *139*, 24–41. https://doi.org/10.1016/j.pocean.2015.07.008

Woodgate, R. A., Aagaard, K., & Weingartner, T. J. (2005). A year in the physical oceanography of the Chukchi Sea: Moored measurements from autumn 1990–1991. *Deep Sea Research Part II: Topical Studies in Oceanography*, *52*(24–26), 3116–3149. https://doi.org/10.1016/j.dsr2.2005.10.016